Compartmentalization of adenosine metabolism in cancer cells and its modulation during acute hypoxia

Karolina Losenkova [1], Mariachiara Zuccarini [1,2], Marika Karikoski[1], Juha Laurila[1], Detlev Boison [3], Sirpa Jalkanen[1], and Gennady G. Yegutkin [1,*]

From the [1]MediCity Research Laboratory, University of Turku, Turku, Finland; [2]Department of Medical, Oral and Biotechnological Sciences, "G. D'Annunzio" University of Chieti-Pescara, Chieti, Italy; [3]Department of Neurosurgery, Robert Wood Johnson and New Jersey Medical Schools, Rutgers University, Piscataway, USA

* To whom correspondence should be addressed: Gennady G. Yegutkin: Medicity Research Laboratory, University of Turku, Tykistökatu 6A, 20520, Finland. genyeg@utu.fi; Tel: +358458775353

JCS Advance Online Article. Posted on 21 April 2020

ABSTRACT

Extracellular adenosine mediates diverse anti-inflammatory, angiogenic and vasoactive effects and becomes an important therapeutic target for cancer, which has been translated into clinical trials. This study was designed to comprehensively assess adenosine metabolism in prostate and breast cancer cells. We identified cellular adenosine turnover as a complex cascade, comprised of (a) the ectoenzymatic breakdown of ATP via sequential nucleotide pyrophosphatase/phosphodiesterase-1, ecto-5'-nucleotidase/CD73 and adenosine deaminase reactions, and ATP re-synthesis through counteracting adenylate kinase and nucleoside diphosphokinase; (b) the uptake of nucleotide-derived adenosine via equilibrative nucleoside transporters; and (c) the intracellular adenosine phosphorylation into ATP by adenosine kinase and other nucleotide kinases. The exposure of cancer cells to 1% O_2 for 24 hours triggered ~2-fold up-regulation of CD73, without affecting nucleoside transporters, adenosine kinase activity and cellular ATP content. The ability of adenosine to inhibit the tumor-initiating potential of breast cancer cells via receptor-independent mechanism was confirmed *in vivo* using a xenograft mouse model. The existence of redundant pathways controlling extracellular and intracellular adenosine provides a sufficient justification for reexamination of the current concepts of cellular purine homeostasis and signaling in cancer.

Keywords: Cancer cells; hypoxia; adenosine metabolism; ecto-5'-nucleotidase/CD73; CD39; adenosine kinase; breast tumor xenograft

The adenosine (ADO) pathway is currently viewed as a significant barrier to the effectiveness of immune therapies and becomes an important therapeutic target in cancer (Boison and Yegutkin, 2019; Vijayan et al., 2017). Most models of cellular ADO turnover depend on interactions between distinct processes including (i) the release of endogenous ATP and other purines, (ii) binding to nucleotide- and adenosine-selective receptors, (iii) ectoenzymatic inactivation of nucleotides and nucleosides, and finally (iv) the re-uptake of nucleotide-derived ADO via equilibrative nucleoside transporters (ENT) and its interconversion into intracellular ATP through complex phosphotransfer reactions (Boison and Yegutkin; Yegutkin, 2008). Extracellular ATP and ADP generally act as potent pro-inflammatory and pro-thrombotic molecules, while ADO has a non-redundant counteracting role in attenuating inflammation and tissue damage (Borea et al., 2018; Bours et al., 2006; Di Virgilio et al., 2018). These effects are primarily mediated through the activation of G-protein-coupled adenosine receptors (A_1, A_{2A}, A_{2B} and A_3), which are selectively co-expressed on vascular endothelial and epithelial cells, lymphocytes, and other cell types (Borea et al., 2018; Jacobson and Muller, 2016). Cancer cells create an immunosuppressive microenvironment through enhanced release of ATP by stressed and apoptotic tumor cells and tumor-infiltrating lymphocytes (Di Virgilio et al., 2018; Maj et al., 2017), and persistent maintenance of high ADO levels in the hypoxic tumor microenvironment (TME) (Ohta et al., 2006; Vaupel and Multhoff, 2017). Because hypoxia and inflammation are interrelated and coincidental processes, enhanced ADO levels in the tumor core might represent an essential pathway driven by hypoxia-inducible factor-1α (HIF-1α) and dampening the excessive inflammatory responses via activation of anti-inflammatory A_{2A} receptors expressed on cytotoxic $CD8^+$ T lymphocytes and other tumor-infiltrating lymphocytes (Bowser et al., 2017; Eltzschig et al., 2012).

In view of opposite, tumor promoting and suppressing, effects of ATP and ADO, substantial attention has been given to the tumorigenic role of key ectoenzymes mediating the sequential conversion of ATP into ADO: nucleoside triphosphate diphosphohydrolase-1 [NTPDase1, also known as Cluster of Differentiation (CD) 39] (Allard et al., 2020; Li et al., 2019), and ecto-5'-nucleotidase/CD73 (Allard et al., 2018; Vijayan et al., 2017). The current view of these ecto-nucleotidases as important anti-cancer targets is based on the premises that the expression levels and activities of CD39 and CD73 are up-regulated on surfaces of vascular endothelial, epithelial, lymphoid and tumor cells as a result of tissue hypoxia, inflammation and oxidative stress (Eltzschig et al., 2003; Eltzschig et al., 2012; Sitkovsky et al., 2014; Vijayan et al., 2017). However, the role of ADO as potential anti-cancer target has not yet been exploited to its fullest therapeutic extent. Specifically, in contrast to traditional paradigms that focus on the CD39-CD73 axis, it has now become clear that other ectoenzymes may contribute to the metabolism of ATP and ADO, including enzymes of the nucleotide pyrophosphatase/phosphodiesterase (NPP) family and tissue-nonspecific alkaline phosphatase (TNAP) (Roberts et al., 2019; Yegutkin, 2008; Zimmermann et al., 2012), adenosine deaminase (ADA) (Spychala, 2000; Yegutkin, 2014), as well as the counteracting ecto-nucleotide kinases, adenylate kinase and nucleoside diphosphokinase (NDPK) (Romani et al., 2018; Yegutkin et al., 2001; Yegutkin et al., 2006). Furthermore, several data provide evidence that, along with

canonical adenosine receptor-mediated pathways, ADO prevents epileptogenesis (Williams-Karnesky et al., 2013), controls vascular inflammation and angiogenesis (Xu et al., 2017), mediates anti-proliferative effects on human lymphocytes (Schiedel et al., 2013), and inhibits the invasion of metastatic cancer cells (Virtanen et al., 2014) via receptor-independent intrinsic mechanisms**.** In particular, the adenosine-removing enzyme adenosine kinase (ADK), which exists in a cytoplasmic (ADK-S) and nuclear (ADK-L) isoform, plays a key role in the regulation of cell proliferation by controlling intracellular ADO homeostasis and intranuclear methylation reactions (Boison, 2013; Williams-Karnesky et al., 2013; Xu et al., 2017). Thus, to understand the role of ADO in cancer, it is important to understand the status of the entire purinome (Boison and Yegutkin, 2019).

Using MDA-MB-231 breast adenocarcinoma cells and PC3 androgen-independent prostate carcinoma cells, this study was undertaken to assess the ADO turnover comprehensively, with the goal to identify a link between extra- and intracellular metabolic pathways and compartmentalization of the ADO system. Because hypoxia, a pathological hallmark of the TME, is known to affect the metabolic profile and energetics of cancer cells, thus worsening disease outcome (Lee et al., 2020; Martinez-Outschoorn et al., 2017), we also evaluated the role of ADO metabolism in tumor growth and adaptation to hypoxia and oxidative stress. We found that the complex interplay of both extrinsic and intrinsic pathways converges into a tightly tuned control of cellular ATP and ADO levels, which provides novel insights into the purinergic mechanisms governing cancer cell metabolism and signaling.

RESULTS

Cancer cells regulate extracellular levels of ATP and ADO via the concerted action of purine-inactivating ectoenzymes and counteracting phosphotransfer reactions

The presence of redundant purine-converting ectoenzymes, which are co-expressed to a variable extent among mammalian cells and tissues and share similarities in substrate specificity (Yegutkin, 2014) implies the necessity to study extracellular purine metabolism as a complex network in each particular cell type. We took advantage of thin layer chromatography (TLC) for the autoradiographic screening of metabolism of radiolabeled nucleotides and ADO in highly invasive cancer cell lines. As shown in **Fig. 1A,** incubation of PC3 prostate cancer (lane 2) and MDA-MB-231 breast cancer (lane 5) cells with [^{3}H]AMP caused its breakdown into [^{3}H]ADO, while the specific inhibitor of CD73, α,β-methylene-ADP (APCP), blocked this reaction (lanes 3 and 6). In the presence of γ-phosphate-donating ATP, a part of [^{3}H]AMP was converted via [^{3}H]ADP into [^{3}H]ATP (lanes 4 and 7), and these reverse phosphoryl transfers can be blocked by Ap_5A (data not shown). Adding [^{3}H]ADP to PC3 (**Fig. 1B**, lane 1) and MDA-MB-231 (lane 4) cells was accompanied by its conversion into [^{3}H]AMP and further to [^{3}H]ADO, which can be prevented by a selective inhibitor of adenylate kinase diadenosine pentaphosphate (Ap_5A, lanes 2 and 5). These data indicate that cancer cells metabolize ADP through adenylate kinase-mediated

transphosphorylation of two ADP molecules into ATP and AMP, rather than "true" nucleotide hydrolase activity. Moreover, the ability of both PC3 (**Fig. 1B**, lane 3) and MDA-MB-231 (lane 6) cells to phosphorylate [^{3}H]ADP into [^{3}H]ATP in an ATP-dependent manner suggests the presence of yet another ecto-nucleotide kinase, NDPK. Data on the ability of PC3 and MDA-MB-231 cells to convert [γ-^{32}P]ATP into AMP and $^{32}PP_i$ also suggests the presence of NPP activity (**Fig. 1C**). For the measurement of ADA activity, we employed [^{3}H]ADO as an initial substrate and a particular solvent system that enabled better separation of ADO and other nucleosides (Yegutkin, 2014). Adding [^{3}H]ADO to the cells triggered its deamination into ^{3}H-labeled inosine and hypoxanthine, which can be prevented by the specific ADA inhibitor EHNA (**Fig. 1D**).

Flow cytometry analysis with anti-CD73, anti-CD39, and anti-NPP1 antibodies ascertained the above radio-TLC data by demonstrating high cell-surface expressions of CD73 and NPP1, but not CD39 (**Fig. 1E**). The cells were also co-stained with anti-CD73 and anti-NPP1 antibodies, together with fluorescently labelled cholera toxin subunit-B (CTB). The latter compound binds to the pentasaccharide chain of ganglioside G_{M1} and is used as a cell-surface marker of glycosphingolipid-rich domains in lymphocytes and other cell types (Janes et al., 1999; Yegutkin et al., 2006). Confocal microscopy analysis confirmed cell surface expression of both CD73 and NPP1 and further demonstrated substantial localization of CD73 within CTB-labeled membrane patches (**Fig. 1F**). Collectively, these data provide evidence that MDA-MB-231 and PC3 cells co-express ADO-producing, ADO-metabolizing and ATP-regenerating ectoenzymes regulating extracellular nucleotide and ADO levels in a coordinated manner. Noteworthy, these cancer cells lack the "classical" ATP-inactivating enzyme NTPDase1/CD39 and instead express NPP1 directly converting ATP into AMP and PP_i.

Cancer cells internalize extracellular ADO and sequentially phosphorylate it via AMP into ADP and ATP through ADK and other nucleotide kinases

To elucidate a link between extra- and intracellular ADO metabolism, PC3 and MDA-MB-231 cells were incubated for 45 min with 10 μM [^{3}H]ADO, washed, lysed and assayed for intracellular ^{3}H-metabolites. TLC analysis has identified ^{3}H-labelled ATP and ADP as major [^{3}H]ADO-derived metabolites, accounting altogether for >90% of total radioactivity (**Fig. 2A**), with a similar pattern of the uptake and phosphorylation of ^{3}H-nucleosides observed during the employment of [^{3}H]AMP as initial substrate (data not shown). Kinetic analysis revealed rather limited capabilities of the cells to take up only a minor portion of [^{3}H]ADO (**Fig. 2B**). The amount of internalized radioactivity was significantly reduced after pretreating the cells with the following compounds prior to addition of [^{3}H]ADO: (a) NBTI and dipyridamole, inhibiting cellular ADO uptake through ENT; (b) excessive amount of unlabeled ADO or its phosphorylated precursor AMP; (c) selective inhibitor of ADA, EHNA; and (d) selective inhibitor of ADK, ABT-702 (**Fig. 2C**). Though, addition of guanosine as an alternative substrate for a more distal enzyme of the purine-inactivating chain, purine nucleoside phosphorylase (PNP), did not affect the flux

of [^{3}H]ADO. No changes were detected in the presence of a non-selective adenosine receptor agonist NECA, indicating that practically all measured radioactivity is due to the transport of [^{3}H]ADO rather than its binding to the cell surface receptors. The employment of 10 μM [^{3}H]AMP as another tracer substrate revealed significantly diminished ability of cancer cells to take up the radioactivity after their pre-treatment with the excessive amounts of unlabelled ADO, AMP, ADP and ATP (but not GMP), as well as with the selective inhibitor of CD73, APCP (**Fig. 2D**). The revealed inhibitory effects are presumably mediated via a dual mechanism, which includes (a) feed-forward inhibition of CD73-mediated [^{3}H]AMP hydrolysis by the precursor nucleotides ATP, ADP, and also APCP (Yegutkin et al., 2001), and (b) the generation of an alternative source of a "cold" ADO pool competing with [^{3}H]ADO for the nucleoside transport systems. Interestingly, pre-treatment of the cells with ABT-702, but not EHNA, was also accompanied by a marked accumulation of intracellular [^{3}H]ADO (**Fig. 2E**). These findings, in conjunction with previous pharmacokinetic data (Boison, 2013), ascertain that ADK (rather than ADA) represents the major metabolic route of intracellular ADO clearance, and further demonstrate that ABT-702 concurrently blocks both cellular uptake of [^{3}H]ADO via ENT and its subsequent ADK-mediated phosphorylation into AMP. In summary, by using a radio-TLC approach, we were able to track major steps of cellular ADO turnover, comprising of (a) metabolism and interconversion of extracellular ATP and other nucleotides through complex ectoenzymatic reactions, (b) the subsequent flux of the nucleotide-derived ADO via ENT, and finally (c) its intracellular interconversion via AMP into ADP and ATP through ADK and other nucleotide kinases (**Fig. 3**).

The effect of acute hypoxia on extracellular and intracellular ADO metabolism.

The following studies were aimed to characterize the effect of acute hypoxia on major pathways involved in metabolism of extracellular ADO. The cells were incubated for 4-24 hours under normoxic (21% O_2) or hypoxic (1% O_2) conditions, with or without a subsequent 1-hour re-oxygenation. CD73 and ADA activities were assayed by TLC using saturating concentrations of [^{3}H]AMP and [^{3}H]ADO as respective enzyme substrates. As shown in **Fig. 4A**, incubation of PC3 and MDA-MB-231 cells in the hypoxic chamber for 24 hours was accompanied by a significantly enhanced rate of [^{3}H]AMP hydrolysis, without affecting the subsequent step of ADA-mediated conversion of [^{3}H]ADO to [^{3}H]inosine. Likewise, a Western blot analysis with an anti-CD73 antibody demonstrated that exposure of cancer cells to 1% O_2 for 24 hours triggers a ~2-fold up-regulation of CD73, which can be restored to control levels by additional re-oxygenation of post-hypoxic cells for one hour (**Fig. 4B**). Confocal microscopy analysis also revealed the enhanced CD73-specific fluorescence in the hypoxia-challenged PC3 and MDA-MB-231 cells, without any changes in the expression of another nucleotide-inactivating ectoenzyme NPP1 (**Fig. 4C** and **Supplementary Fig. S1**).

For evaluating intracellular ADO metabolism, the cells were incubated for 4-24 hours in a hypoxic chamber with or without 1-hour of re-oxygenation, and subsequently incubated for 45-min with 10 μM

[^{3}H]ADO. The relative proportions of cell-incorporated [^{3}H]ADO and its phosphorylated ^{3}H-metabolites were analyzed chromatographically, using autoradiographic imaging (**Fig. 5A**) or scintillation β-counting (**Fig. 5B-D**). Acute hypoxia did not affect the total amount of radioactivity taken up by the cells (**Fig. 5B**). However, incubation of the cells in the hypoxic chamber for 24 hours was accompanied by their diminished ability to phosphorylate [^{3}H]ADP into [^{3}H]ATP (**Fig. 5C**), with respective accumulation of [^{3}H]ADP as an intermediate metabolite (**Fig. 5D**). Collectively, these data suggest that exposure of cancer cells to hypoxia inhibits local ATP synthesis/replenishment via extra-mitochondrial salvage pathway (presumably due to hypoxia-driven down-regulation of cytosolic NDPK (Rasool et al., 2017)) and concurrently triggers up-regulation of CD73, without affecting nucleoside transport system and other enzymes of ADO metabolism, NPP1, ADA and ADK.

Acute hypoxia does not affect ADK expression, cellular ATP content, and cytoskeletal structure of cancer cells

In a different set of experiments, normoxic and hypoxic cancer cells were co-stained with antibodies against HIF-1α and ADK. Exposure of PC3 and MDA-MB-231 cells to hypoxia triggered marked up-regulation of HIF-1α, whereas the distribution of ADK in control and hypoxia-challenged cells revealed fairly comparable staining patterns, with bright punctate cytosolic fluorescence observed in all cancer cells studied (**Fig. 6A** and **Supplementary Fig. S2**). Additional Western blot analysis confirmed the co-expression of the two ADK isoforms, with no differences in the expression levels of ADK-S and ADK-L between control and hypoxic cells (**Fig. 6B** and **Supplementary Fig. S3**). Direct bioluminescent analysis also did not reveal any hypoxia-induced changes in global cellular ATP content (**Fig. 6C**). For visualization of putative cellular ATP stores, we employed a selective fluorescent ATP sensor-1 (AS1) (Losenkova et al., 2018; Xu et al., 2009). AS1-loaded PC3 cells were co-stained with the cell-surface marker Alexa555-CTB and the actin-binding drug Alexa488-Phalloidin. Computer reconstructions from serial confocal images along the *z*-axis revealed that AS1 fluorescence in PC3 cells is mainly accumulated within granular vesicles beneath CTB-labeled patches and also display more diffuse cytoplasmic staining in the perinuclear regions (**Supplementary Fig. S4** and **Movie S1**). Comparative quantitative analysis of maximum intensity projection demonstrated that incubation of PC3 and MDA-MB-231 cells in the hypoxic chamber for 24 hours did not affect AS1-specific fluorescence (**Fig. 6D** and **Supplementary Fig. S5**). These data demonstrate that acute hypoxia does not affect global ATP content and also releasable ATP stores in the cancer cells studied. Moreover, exposure of PC3 and MDA-MB-231 cells to hypoxia also did not cause any derangement of the major cytoskeletal elements, with fairly comparable organization of F-actin in a thick cortical ring and in fine filaments (**Supplementary Fig. S2)** and well-organized cytoplasmic filamentous structures and microtubule networks (**Supplementary Fig. S5**) determined both in normoxic and hypoxic cells.

Pre-treatment of MDA-MB-231 breast tumor xenografts with ADO inhibits tumor growth in vivo

To evaluate the therapeutic significance of our observations, luciferase-expressing MDA-MB-231-luc-D3H2LN cells were pretreated with exogenous ADO, and subsequently inoculated into mammary fat pads of severe combined immunodeficiency (SCID) female mice. Luciferase reporter allowed us to monitor the rate of tumor growth as a function of time, which can be divided into three major phases: (a) partial decrease in the bioluminescence signal during the first four days (presumably reflecting the elimination of a certain portion of the inoculated cells during their dissemination and adaptation to the foreign soil); (b) relatively slow but progressive tumor growth within the next two weeks; and (c) rapid exponential growth of the established tumor reaching the volume of ~600 mm^3 at day 32, with obvious signs of tissue necrosis (**Fig. 7** and **Supplementary Figs. S6 and S7**). The latter stage is also characterized by the ability of tumor to recruit and expand new blood vessels (see below), and spontaneous development of secondary lung metastases (data not shown).

Given the ability of cancer cells to efficiently metabolize ADO, the cells were pre-treated with a relatively high concentration of ADO (100 μM), which is higher than in the above *in vitro* cell culture assays. The dynamics of tumor growth was periodically monitored by bioluminescence imaging and normalized relatively to day 4. Strikingly, ADO-treated cancer cells showed delayed onset of tumor formation with a significant lag-phase in their growth on days 7 and 11 (**Fig. 7A,C).** In contrast, the non-selective adenosine receptor agonist NECA did not affect the initial steps of tumor growth and dissemination (**Supplementary Fig. S6**). In the second set of experiments, ADO or NECA were injected directly into the established tumors starting from day 22. However, no differences in the bioluminescence signals, tumor volumes or weights were detected among the control and treatment groups (**Fig. 7** and **Supplementary Fig. S7**).

After the last imaging on day 32, the mice were euthanized and tumors excised and processed for histochemical analysis, as described in Materials and Methods. Lead nitrate-based enzyme histochemistry revealed the presence of high ATPase activities on the host-derived vascular blood vessels and connective tissues, while AMPase was primarily associated with MDA-MB-231 xenografts, with less intense AMP-specific brown staining being also detected in blood vessels, but not in tumor-surrounding stroma (**Fig. 8A**). Measurement of TNAP activity by using the artificial chromogenic substrate BCIP/NBT revealed the abundant enzyme expression in large blood vessels, and more faint and diffuse blue staining throughout the whole tumor xenograft (**Fig. 8A**). Additional immunofluorescence staining confirmed the abundant cell-surface expression of CD73 on human breast cancer cells, and further demonstrated that mouse CD73 is primarily associated with SMA-positive vascular smooth muscle cells (**Fig. 8B**). Yet another mouse ecto-nucleotidase, CD39, was selectively localized on CD31-positive vascular endothelium (**Fig. 8C**), while intracellular ADK was ubiquitously expressed both by blood vessels and tumor cells (**Fig. 8D**). Together, these data provide the proof-of-principle that ADO may inhibit the tumor-initiating potential of breast cancer cells *in vivo* without affecting their growth at more advanced

stages of tumorigenesis, and further suggest the existence of a complex cross-talk between tumor- and host-derived enzymes coordinately regulating cellular ATP and ADO levels within the TME.

DISCUSSION

The aim of this study was to provide a comprehensive analysis of cellular ADO turnover in highly invasive prostate and breast cancer cells and on this basis, to identify a link between ADO metabolism and the ability of cancer cells to maintain high plasticity and growth potential during oxygen deprivation and in tumor-host interactions. Major findings of this paper are summarized as follows: (1) cancer cells co-express a broad spectrum of enzymes capable of regulating, in conjunction with nucleoside transporters, the active cycling between extracellular and intracellular ATP and ADO pools in a coordinated fashion; (2) the exposure of cancer cells to short-term hypoxia triggers selective up-regulation of CD73 without affecting other ectoenzymes and the "intrinsic components" of the purine turnover cascade; (3) ADO also inhibits the tumor-initiating potential of breast tumor xenografts *in vivo* without affecting their growth at more advanced stages of tumorigenesis.

The role of ADO in cancer has been extensively investigated, leading to the deduction of its crucial roles in immunomodulation, angiogenesis and blood flow distribution (Borea et al., 2018; Jacobson and Muller, 2016; Vijayan et al., 2017). Most recent work has focused on the development of clinical approaches to treat cancer by antibodies targeting the activities of CD39 and CD73, and also A_{2A} receptor blockers, which have been heralded as promising therapeutic immune-checkpoint targets (Allard et al., 2020; Chen et al., 2019; Li et al., 2019; Sitkovsky et al., 2014). However, major gaps in knowledge that impede the development of effective ADO-based therapeutics include: (a) lack of consideration of the redundancy of ectoenzymatic pathways orchestrating balanced ATP and ADO levels; and (b) focus on extracellular ADO without consideration of intracellular ADO metabolism (Boison and Yegutkin, 2019). By using a radio-TLC approach in combination with immunofluorescence and immunoblotting analyses, we were able to track all major steps of cellular purine turnover, which include (a) the ectoenzymatic breakdown of ATP via sequential NPP1, CD73, ADA and PNP reactions, (b) ATP re-synthesis through adenylate kinase and NDPK reactions, (c) the subsequent uptake of nucleotide-derived ADO via ENT, and finally (d) the intracellular interconversion of ADO via AMP into ADP and ATP through ADK and other nucleotide kinases (**Fig. 3**).

Contrary to the previously reported exclusive role of NTPDase1/CD39-mediated ATP hydrolysis via ADP into AMP by vascular endothelial cells (Robson et al., 2005; Yegutkin et al., 2011; Yegutkin et al., 2001), MDA-MB-231 and PC3 cells express an additional ectoenzyme, NPP1, capable of converting ATP into AMP and PP_i (see **Fig. 1**). These findings are consistent with recent data showing the expression of NPP1 on different cancer cells and tumor tissues (Lau et al., 2013; Roberts et al., 2019), and also supported by early observations on the ability of cancer cells, but not vascular endothelial cells and lymphocytes, to generate and maintain in their vicinity another physiologically important by-product of

NPP reaction, PP_i (Helenius et al., 2012). The identification of the NPP1-CD73 axis as an alternative CD39-independent adenosinergic loop implies that tumors might have the capability to bypass CD39-based cancer therapeutics. It is also pertinent to note that a broadly employed class of synthetic analogues of PP_i, bisphosphonates, has been widely used for the treatment of malignancies associated with bone metastasis in breast and prostate cancers (Cremers et al., 2019; Orriss et al., 2016). Given that some non-nitrogen containing bisphosphonates (clodronate, etidronate and tiludronate) can substitute for PP_i by metabolic incorporation into non-hydrolysable ATP analogues (Cremers et al., 2019), it would be attractive to hypothesize that anti-tumor effects of these drugs are defined, at least in part, by interference with the function of NPP1 and other enzymes involved in extracellular ATP and PPi homeostasis.

We have also identified ecto-adenylate kinase and NDPK as important effector systems for local scavenging of extracellular nucleotides. A cell surface-localized isoform of adenylate kinase-1 (Dzeja and Terzic, 2003; Yegutkin, 2008; Yegutkin et al., 2006) and enzymes of the NDPK/NME/NM23 family (Romani et al., 2018; Yokdang et al., 2015) are expressed in various types of malignant and non-cancerous cells, where they are implicated through multiple mechanisms in different processes, including cell proliferation and differentiation, and tumor metastasis. Under normal physiological conditions, the ecto-nucleotide kinases seem not to compete with ecto-nucleotidases for a limited pool of the released nucleotide substrates (Yegutkin, 2008). However, in the settings of inflammation, hypoxia and oxidative stress, intratumoral levels of ATP can be increased up to 10^{-5}-10^{-4} mol/L (Di Virgilio et al., 2018; Maj et al., 2017). Acute changes in the specific ratios of nucleoside tri-, di- and monophosphates, in conjunction with feed-forward inhibition of CD73 activity by precursor ATP/ADP (Yegutkin et al., 2001), should determine the directional shift from a nucleotide-inactivating pathways towards reverse ATP re-synthesis in the TME. Thus, the co-expression of NPP1, CD73 and counteracting ecto-nucleotide kinases may represent a novel and currently neglected route contributing to the active cycling between ATP, ADP and ADO on the surface of malignant cells devoid of NTPDase1/CD39.

Our work also points to the existence of a highly dynamic exchange of ATP and ADO between extra- and intracellular compartments. Cancer cells are capable of replenishing the intracellular pool of nucleotides by taking up a certain amount of ADO through ENTs and its sequential conversion into ATP. This catalytic cascade is initiated via ADK-mediated phosphorylation of ADO into AMP rather than its deamination to inosine, as ascertained by markedly diminished intracellular conversion of [^{3}H]ADO into high-energy ^{3}H-phosphoryls in the presence of the ADK inhibitor ABT-702, but not the ADA inhibitor EHNA (see **Fig. 2E**). These data are consistent with the current view that, under baseline conditions, ADK (specifically, the ADK-S isoform) is the predominant route for the metabolic clearance of ADO, with the goal to keep ADO levels low (Boison, 2013; Boison et al., 2010). However, the low affinity, high capacity enzyme ADA may also assist in the metabolic clearance of ADO, especially under pathological states, when ADO levels are supra-physiological and the capacity of ADK is exceeded (Spychala, 2000). The generated AMP in turn serves as an intermediate metabolite, which is rapidly

phosphorylated into ADP and ATP via spatially arranged phosphotransfer networks comprised of cytosolic adenylate kinase and NDPK (Dzeja and Terzic, 2003; Romani et al., 2018).

In view of the emerging regulatory role of hypoxia in tumorigenesis (Eltzschig et al., 2012; Lee et al., 2020), we next compared the pattern of cellular ADO turnover in normoxic versus hypoxic cancer cells. Acute hypoxia triggered significant up-regulation of the key hypoxia-driven transcriptional target HIF-1α and also CD73, without any shifts in the expression levels and activities of other enzymes of the purine-inactivating chain, NPP1 and ADA. These findings are consistent with previous data on the enhanced CD73 activity following the exposure of endothelial, epithelial, and tumor cells to short-term hypoxia (Allard et al., 2018; Eltzschig et al., 2003; Eltzschig et al., 2012; Ledoux et al., 2003; Sitkovsky et al., 2014; Synnestvedt et al., 2002), and also supported by early studies, which identified a hypoxia-responsive element in the promoter of the CD73 (Nt5e) gene and demonstrated that CD73 is a transcriptional factor of HIF-1α (Synnestvedt et al., 2002). On the other hand, the activities of CD73 and other ecto-nucleotidases can be down-regulated on vascular and microvascular endothelium and other cell types during chronic oxygen deprivation (Yegutkin et al., 2011), at sites of transplantation (Robson et al., 2005), atherogenesis (Mercier et al., 2012), and also arterial (Roy et al., 2018) and pulmonary (Visovatti et al., 2016) hypertension. These different, often opposite, cellular responses to acute and chronic hypoxia, as well as ischemia should be taken into account during the development of pharmacological and metabolic treatments against the proliferation of cancer cells and other energy-depleting conditions associated with hypoxia, neovascularization and inflammation.

Hypoxia may also affect the “intrinsic part” of the purine turnover cascade. Previous data on significant down-regulations of key ADO-metabolizing enzymes, ADK (Chen et al., 2018; Pignataro et al., 2008) and ADA (Kobayashi et al., 2000), and the diminished expression of ENT1 (Casanello et al., 2005; Chen et al., 2018; Eltzschig et al., 2005; Kobayashi et al., 2000) in vascular endothelial and other cells subjected to hypoxia suggested the accumulation of ADO both in the extracellular milieu and inside the hypoxic cells. On the other hand, the treatment of MDA-MB-231 cells for 24 hours with 1% O_2 had no effect on downstream expression and function of human ENT1 and ENT2 (Krys et al., 2019). Our data also indicate that hypoxia does not affect the nucleoside transport and the ensuing step of ADK-mediated [^{3}H]ADO phosphorylation in cancer cells. Interestingly, contrary to the previously reported insufficient ATP production in vascular endothelial cells subjected to hypoxia (Losenkova et al., 2018; Turner et al., 2004), exposure of cancer cells to hypoxia was not accompanied by depletion in global cellular ATP content and putative releasable ATP stores (see **Fig. 6**). These apparent discrepancies may be defined by the high plasticity of epithelial-derived carcinoma cells capable to re-wire metabolic processes through a compensatory HIF-1α-induced increase in autophagy, mitophagy, glucose uptake and glycolysis (Lee et al., 2020; Martinez-Outschoorn et al., 2017). At the same time, hypoxic cancer cells may reduce their metabolic demands by decreasing flux through the tricarboxylic acid cycle in mitochondria (Carling, 2017; Lee et al., 2020; Martinez-Outschoorn et al., 2017), as well as via hypoxia-driven down-regulation of the cytosolic NDPK (Rasool et al., 2017) with respective inhibition of the local

synthesis/replenishment of ATP via extra-mitochondrial nucleotide salvage pathway (present study). In fact, by adapting their metabolic apparatus to hypoxia, oxidative stress and nutrient deprivation, and by maintaining high cellular ATP, cancer cells would gain an advantage for suppressing the host's immune defense and promoting angiogenesis in the TME.

To evaluate the potential therapeutic potential of ADO treatment, we studied its efficiency in SCID mice bearing tumor xenograft by using *in vivo* imaging techniques. Treatment of breast cancer cells with micromolar concentrations of ADO (but not with the non-selective adenosine receptor agonist NECA) significantly inhibited their tumor-initiating potential, without affecting the growth of the established tumor at more advanced stages of tumorigenesis. These data are consistent with previous observations showing the ability of micromolar concentrations of ADO, but not NECA, to inhibit the invasion of MDA-MB-231 and PC3 cells *in vitro* via non-cytotoxic and receptor-independent mechanism (Virtanen et al., 2014). Further studies would be required to elucidate the intrinsic mechanisms of the anti-tumor action of ADO, which can fall into two main categories: (i) A role that is linked to the intracellular uptake and phosphorylation of ADO, with subsequent deregulation of AMP-activated protein kinase (AMPK) and related signaling pathways (Carling, 2017; Virtanen et al., 2014), and (ii) a specific, emerging role of an isoform of ADK, which is expressed in the cell nucleus (ADK-L) and acts as epigenetic regulator (Boison et al., 2002; Boison and Yegutkin, 2019; Williams-Karnesky et al., 2013; Xu et al., 2017). Additional histochemical analysis confirmed histopathological diversity of the TME and further demonstrated selective localization of purine-converting enzymes on normal host cells and the aberrant malignant cells. Specifically, data on the presence of high CD73-mediated AMPase activity in tumor xenografts (see **Fig. 8**) are in line with the current view of CD73 as a poor prognostic biomarker for clinical outcomes in a wide spectrum of tumor types (Allard et al., 2018; Vijayan et al., 2017). Furthermore, selective expression of NTPDase1/CD39 in the tumor vasculature and supporting stroma (**Fig. 8**), and also in tumor-infiltrating lymphocytes (Allard et al., 2020; Li et al., 2019; Maj et al., 2017), could represent an important effector system for local inactivation of pro-inflammatory ATP in the vicinity of tumor cells devoid of CD39.

In conclusion, the identification of cellular ADO turnover as a complex network comprised of highly dynamic and apparently interrelated extra- and intracellular pathways and its modulation in response to acute hypoxia provides significant justification for the re-examination of the role of purinergic machinery in the maintenance of the high plasticity of cancer cells and their adaptation to oxygen deprivation and other energy-depleting conditions. The directional manipulation of the ATP-ADO axis in cancer cells has recently evolved into novel therapeutic approaches, particularly focused on the development of small-molecule inhibitors and antibodies directed against CD39 and/or CD73, in combination with $A_{2A}R$ blockers and other immune checkpoint inhibitors (Allard et al., 2020; Chen et al., 2019; Li et al., 2019; Vijayan et al., 2017). Other therapeutic strategies alleviating immunosuppressive and tumorigenic activities of ADO may include supplementation of oxygen via respiratory hyperoxia to reduce intratumoral hypoxia (Hatfield et al., 2015), as well as the directional manipulation of extra- and

intracellular pH homeostasis in the TME (Vaupel and Multhoff, 2017). The realization that ADO metabolism in cancer cells is more complex than previously recognized justifies an armamentarium of different agents, which could significantly improve the efficacy of ongoing clinical trials. In particular, the following strategies might help to prevent ADO-mediated antitumor immune activities and enable tumor regression: (1) the development of small-molecule inhibitors against NPP1 and TNAP (Channar et al., 2018; Lee and Muller, 2017), with the desired outcome to prevent ADO formation via alternative ADO-producing pathways; (2) suppression of tumor growth and metastasis via modulation of extracellular ATP re-synthesis through reverse phosphotransfer reactions (Romani et al., 2018; Yokdang et al., 2015); and (3) directional manipulation of intracellular ADO metabolism using selective ADK inhibitors (Toti et al., 2016), which may permit the regulation of ADO levels in a compartment-selective manner. It is important to emphasize that cancer cells might be flexible enough to utilize alternative routes of ADO production, thereby compromising the efficacy of currently proposed therapeutics. A more comprehensive approach of targeting purine metabolism in cancer appears warranted, making use of combination therapies to target several key steps in purine metabolism synergistically.

MATERIALS AND METHODS

Reagents and antibodies

The following mouse monoclonal antibodies (mAbs) were used in this study: anti-β-tubulin (clone TUB2.1, Sigma-Aldrich), anti-HIF-1α (clone H1alpha67, ThermoFisher), anti-NPP1 (CD203a/PC-1, clone 3E8, gift of Prof. Fabio Malavasi) (Horenstein et al., 2013), anti-CD73 (4G4) and isotype-specific mAb against chicken T-cells (3G6) (Losenkova et al., 2018), Alexa Fluor® 488-conjugated anti-smooth muscle actin-α (SMA-α, Sigma Aldrich). Polyclonal rabbit anti-human CD73 (h5NT-1_L) and guinea pig anti-human NTPDase1/CD39 (hN1-1_C) antibodies, as well as pre-immune sera from the same animals were provided by Prof. Jean Sevigny (http.//ectonucleotidases-ab.com). Rabbit anti-CD73 (D7F9A) mAb was from Cell Signaling Technology®, and polyclonal rabbit anti-ADK Ab, produced in house from recombinant ADK. Polyclonal serum was found to be highly specific for both isoforms of ADK, as determined in a Western blot analysis performed on liver extracts from Adk-/-, Adk+/-, and Adk+/+ mice (Boison et al., 2002). Chicken polyclonal anti-vimentin and Alexa Fluor® 488-conjugated rat anti-mouse CD31 antibodies were from BioLegend Inc (San Diego, CA). Rat anti-mouse CD73 Ab (clone TY/23) was from BD Biosciences. Secondary Allophycocyanin (APC)-conjugated and Alexa Fluor® 488-, 546- and 633-conjugated goat anti-mouse, anti-rabbit, anti-chicken and anti-rat antibodies, Alexa Fluor®488- and 546-conjugated Phalloidin, Alexa Fluor®555-conjugate of CTB from *Vibrio cholera*, ProLong® Gold Antifade reagent without and with 4,6-diamidino-2-phenylindole (DAPI), 5'-bromo-4-chloro-3-indolyl phosphate (BCIP), and nitro blue tetrazolium (NBT) were from Invitrogen™ (ThermoFisher Life

Technologies). Cy™3-conjugated donkey anti-guinea pig IgG was from Jackson Immuno Research Laboratories (West Grove, PA). IRDye® 680RD infrared dye-conjugated donkey anti-rabbit and anti-mouse immunoglobulins were from LI-COR Biosciences GmbH. A selective pincer-like benzene-bridged fluorescent ATP sensor-1 (AS1) originally synthesized and defined as "C*ompound 1*" (Xu et al., 2009) was provided by Drs. Zhaochao Xu and Juyoung Yoon. [2,8-^{3}H]ADP and [γ-^{32}P]ATP were from Perkin Elmer (Boston, MA). [2,8-^{3}H]AMP and [2,8-^{3}H]ADO were from American Radiolabeled Chemicals Inc. (Campro Scientific, The Netherlands). Dipyridamole, S-(4-nitrobenzyl)-6-thioinosine (NBTI), 5'-N-ethyl-carboxamide-adenosine (NECA), erythro-9-(2-hydroxy-3-nonyl)adenine (EHNA), APCP, ABT-702, Ap_5A, non-labelled nucleotides and nucleosides, and other chemicals were from Sigma-Aldrich**.**

Cell culture and hypoxia treatment

The PC3 human prostate carcinoma cell line and the MDA-MB-231 human breast adenocarcinoma cells were purchased from ATCC (Manassas, USA). The cells were maintained in 75 cm^2 tissue culture flasks at 37°C in a humidified atmosphere of 5% CO_2/95% air in Gibco Ham's F-12K medium (PC3) or high glucose Dulbecco's modified Eagle-Medium (DMEM) (MDA-MB-231) supplemented with 10% heat-inactivated fetal calf serum (FCS), 100 U/mL penicillin and 100 µg/mL streptomycin. For treatment experiments, the cells were harvested with trypsin/EDTA and seeded onto appropriate tissue culture plates for 24-48 hours to reach confluence. The complete medium was replaced then by RPMI-1640 containing 25 mM HEPES (pH 7.35) and 1% FCS (RPMI/FCS). The cells were incubated at 37˚C for 4-24 hours in the humidified hypoxic chamber containing 1% O_2 (Biotrace Ruskinn InvivO2 Hypoxia Workstation C400/C Plus) and then either processed immediately for enzymatic and other assays ("*hypoxic cells*") or additionally gassed in a humidified atmosphere of 21% O_2 prior to the experiments ("*hypoxia-reoxygenation*" treatment). Control cells (defined as "*normoxic*") were placed in a conventional incubator for the same periods of time. Importantly, in the case of hypoxia experiments, all assays were conducted directly in the chamber through the tightly adjusted sleeves to avoid reo-oxygenation.

TLC analysis of extracellular purine metabolism

PC3 and MDA-MB-231 cells were seeded overnight onto 96-well flat bottom clear plates at a density of 10000 cells per well. Ectoenzymatic activities were determined by incubating the adherent cells with radiolabeled and unlabeled substrates at 37˚C in a final volume of 100 µl RPMI/FCS medium in the following ways: (i) nucleotide-converting pathways were evaluated by incubating the cells for 45 min with 20 µM [^{3}H]ADP or 100 µM [^{3}H]AMP in the absence and presence of γ-phosphate-donating ATP (300 µM); (ii) ADA activity was determined by incubating the cells for 60 min with 50 µM [^{3}H]ADO; (iii) the cells were also incubated for 20 min with 10 µM [γ-^{32}P]ATP. In some competitive assays, the samples were pretreated with specific inhibitors of adenylate kinase (Ap_5A, 100 µM), eN/CD73 (APCP, 100 µM) and ADA (EHNA, 10 µM) for 30 min prior to addition of ^{3}H-substrates. Aliquots of the mixture were applied onto Alugram® SIL G/UV_{254} (in the case of ^{3}H-labeled compounds) or Polygram® CEL-

300 PEI (for [γ-^{32}P]ATP assays) TLC sheets (Machery-Nagel, Duren, Germany), separated using appropriate solvent systems and developed by autoradiography using Kodak BioMax MS films (Carestream, Rochester, NY). To study the effect of hypoxia on specific eN/CD73 and ADA activities, the cells were subjected to normoxia, hypoxia and re-oxygenation and subsequently incubated for additional 60 min with 300 μM [^{3}H]AMP or [^{3}H]ADO, as respective enzyme substrates. ^{3}H-labeled AMP, ADO, inosine and hypoxanthine were separated by TLC and quantified by scintillation β-counting, as described earlier (Yegutkin, 2014; Yegutkin et al., 2001).

TLC analysis of intracellular purine metabolism

Cancer cells were seeded onto 24-well tissue culture plates at a density of ~60,000 cells/well and cultured overnight in a complete medium, which was then replaced by 340 μl RPMI/FCS. Cells were subjected to the following treatments: 1) pre-incubation for 45 min at 37˚C with the following drugs: inhibitors of nucleoside transport NBTI and dipyridamole (final concentration 50 nM for both), inhibitor of ADA (EHNA, 10 μM), inhibitor of CD73 (APCP, 100 μM), inhibitor of ADK (ABT-702, 500 nM), non-selective agonist of adenosine receptors (NECA, 25 μM), as well as unlabeled ATP, ADP, AMP, ADO, GMP or guanosine (250 μM each); 2) exposure to acute hypoxia with or without subsequent re-oxygenation. The treated cells were incubated for 45 min at 37˚C with different concentrations of [^{3}H]AMP or [^{3}H]ADO in a final volume of 360 μl (~0.8×10^{6} dpm/well for both radiotracers), washed with PBS to remove non-bound radioactivity and lysed in the appropriate mammalian cell lysis buffer (Perkin Elmer). Aliquots of the lysates were separated by TLC and then either developed by autoradiography or quantified for the relative amounts of cell-incorporated ^{3}H-metabolites, as described above.

Immunofluorescence staining of the cells

Cancer cells grown on 13-mm coverslips in 24-well plates were subjected to hypoxia as specified above. The treated cells were washed with PBS and immediately fixed for 5 min with PBS containing 4% paraformaldehyde. The adherent fixed cells were processed directly for staining of membrane-bound nucleotidases or additionally permeabilized for 3 min with 0.2% Triton X-100 for intracellular staining, as described earlier (Losenkova et al., 2018). Alexa Fluor® 546- and 488-conjugated Phalloidin (1 μg/ml), Alexa Fluor® 555-conjugated CTB (0.5 μg/ml) and ATP-sensing fluorescent dye AS1 (40 μM) were added during the incubation with secondary fluorescently-labelled antibodies for labelling the filamentous actin, plasma membrane microdomains, and putative ATP stores, respectively. The coverslips were mounted with ProLong® medium without or with DAPI and examined using a 3i spinning disk confocal microscope CSU-W1 with Photometrics Evolve EM-CCD camera, and Slidebook 6.0 software (Intelligent Imaging Innovations, Inc.). Z-stacks of normoxic and hypoxic cells were captured using C-Apochromat 40×/1.1 or Plan-Neofluar oil 63×/1.4 objective (Carl Zeiss) at identical exposure times for

each antibody. Maximum intensity projection of a confocal z-stack for each channel for prepared and analyzed in parallel by using Imaris 8.4 (Bitplane) and ImageJ 1.52a software (Schneider et al., 2012).

Flow Cytometry

Control and hypoxia-exposed cells grown in 24-well plates were detached by trypsin/EDTA and subsequently incubated with appropriate primary and secondary fluorochrome-conjugated antibodies diluted in PBS buffer containing 2% FCS and 0.01% NaN_3. Flow cytometry analyses were performed using BD LSRFortessa (BD Biosciences) and analyzed using FlowJo (TreeStar) software.

Western blotting

Control and hypoxic cancer cells grown in 6-well plates were lysed and loaded on a 10% SDS-polyacrylamide gel (~25 µg protein/lane), as described earlier (Virtanen et al., 2014). After electrophoresis, proteins were transferred to nitrocellulose blotting membrane (Amersham) followed by immunoblotting with anti-CD73 (D7F9A) and anti-ADK antibodies, as well as anti-β-tubulin mAb as a control for protein loading. Signals were detected using appropriate IRDye® 680RD-conjugated secondary antibodies and Odyssey® CLX-1005 infrared imaging system (LI-COR Biosciences GmbH). Protein and ATP concentrations in cell lysates were determined using the BCA Protein Assay Kit (Pierce, Rockford, IL) and luciferin-luciferase kit ATPLite (Perkin Elmer), respectively. All measurements were performed with Tecan Infinite M200 microplate reader (Salzburg, Austria).

Human breast tumor xenograft experiments

Luciferase-expressing adenocarcinoma cell line, MDA-MB-231-luc-D3H2LN, was from Caliper Life Sciences. This clonal line was derived from human MDA-MB-231 cells by stable transfection for the North American Firefly Luciferase gene expressed from the SV40 promoter. In the first study, MDA-MB-231-luc-D3H2LN cells were pre-treated overnight with 100 µM ADO or 10 µM NECA. Vehicle-treated cells contained DMEM-based complete medium without or with 0.02% DMSO. On the next day, the cells were detached, additionally treated for 15 min at room temperature with vehicle or equimolar concentrations of ADO and NECA, and immediately inoculated into the fourth mammary fat pads (10^6 cells in 50 µl PBS) of ten-week-old female SCID mice (CB17/lcr-Prkdc scid/Crl, Charles River, Germany). Tumor growth was optically imaged by IVIS50 (IVIS-Spectrum Imaging System, Caliper Life Sciences), after a substrate D-luciferin injection. In the second set of orthotopic experiments, MDA-MB-231- luc-D3H2LN xenografts were allowed to grow for three weeks, and subsequently treated with 50 µl of ADO (100 µM), NECA (10 µM) or equal volumes of DMSO or PBS, injected intratumorally at days 22, 26 and 29 post-inoculation. On day 32, the mice were sacrificed and the tumors were excised, weighted using precision scales (Mettler Toledo), measured using an electronic caliper (Mitutoyo), and processed for further histological analysis. Tumor volume was calculated according to the formula $V = (\pi/6)(d1 \times d2 \times d3)$, where d1—d3 are perpendicular tumor diameters (width, length, height). All mouse

experiments were carried out at the Central Animal Laboratory of the University of Turku, Finland according to the European Convention for the Protection of Vertebrate Animals used for experimental and other Scientific Purposes, and the Statutes 1076/85 and 1360/90 of The Animal Protection Law in Finland and EU Directive 86/609. Animal welfare was monitored daily for clinical signs. The experimental procedures were reviewed by the local Ethics Committee on Animal Experimentation of the University of Turku and approved by the Provincial State Office of Western Finland with the license ID ESAVI/5587/04.10.07/2014.

Tumor histochemistry

The excised tumors were embedded in the cryo-mold with Tissue-Tek® O.C.T. compound (Sakura Finetek), cut at 10 μm onto superfrost glass slides, and processed for enzyme histochemistry and immunofluorescence staining, as described elsewhere (Losenkova et al., 2020). Briefly, ecto-nucleotidase activities were assayed by incubating tissue slices in trizma-maleate sucrose buffer (TMSB, pH 7.3) at 37°C with 400 μM ATP (for 30 min) or AMP (15 min) in the presence of $Pb(PO_4)_2$, followed by microscopic detection of the nucleotide-derived P_i as a brown precipitate. The activity of TNAP was measured by incubating the slides for 30 min in TMSB (pH 9.0) containing the artificial chromogenic enzyme substrates BCIP/NBT (400 μM each), and subsequent monitoring the blue color reaction. Multiple bright-field images of adjacent tissue areas were captured using Pannoramic-250 Flash slide scanner (3DHistech Ltd., Budapest, Hungary), and further stitched to a larger overview using the accompanying Pannoramic Viewer 1.15.4 software. For the immunofluorescence analysis, tumor sections were incubated overnight at +4ºC in Shandon Sequenza Staining System (Thermo Scientific) with antibodies against different human and mouse enzymes (CD73, CD39 and ADK, all diluted at 1:300), washed, and subsequently incubated for one hour at room temperature with isotype-matched fluorochrome-conjugated second-stage immunoglobulins. Alexa Fluor® 546 Phalloidin and Alexa Fluor® 488-conjugated SMA and CD31 were added during the incubation with secondary fluorescently-labelled antibodies for labelling the filamentous actin, smooth muscle cells, and blood vessels, respectively. The slides were mounted with ProLong® medium with DAPI and examined using a laser scanning confocal microscope Zeiss LSM880 with Plan-Neofluar 20×/0.8 objective (Carl Zeiss) or a 3i spinning disk confocal microscope CSU-W1 with C-Apochromat 40×/1.1 objective, as described above.

Statistical analysis

Statistical significance was determined by using two-tailed Student´s t-test and Mann-Whitney U-test. The maximum [^{3}H]ADO-binding capacities of the cells (B_{max}) were determined using nonlinear least-squares curve fitting. In the case of mouse xenograft experiments, statistical significance between the control and treated groups was determined by multiple t-test grouped analysis using the Holm-Sidak method. The statistical significance levels were denoted as *P<0.05. All results were analyzed with Prism GraphPad 7 software (GraphPad, San Diego, CA).

Abbreviations:

ADK, adenosine kinase; ADO, adenosine; APCP, α,β-methylene-ADP; Ap_5A, dinucleotide pentaphosphate; CD73, ecto-5'-nucleotidase/CD73; NDPK, nucleoside diphosphokinase; NPP, nucleotide pyrophosphatase/ phosphodiesterase; NTPDase, nucleoside triphosphate diphosphohydrolase; TLC, thin-layer chromatography; TME, tumor microenvironment.

Acknowledgments

We thank Dr. Jouko Sandholm at the Cell Imaging and Cytometry Unit of Turku Bioscience Centre for microscopy support and Biocenter Finland for microscopy and flow cytometry equipment. We are also grateful to Drs. Petra Miikkulainen and Heidi Högel for help with hypoxic chamber experiments, Dr. Jean Sevigny for providing the antibodies against human and mouse CD73 and CD39, Dr. Fabio Malavasi for providing anti-NPP1 antibodies, and Drs. Zhaochao Xu and Juyoung Yoon for providing the ATP sensor AS1.

Competing interests

The Authors declare that there are no competing or financial interests associated with the manuscript.

Funding

This work was supported by grants from the Sigrid Juselius Foundation and the National Institutes of Health, USA (NS065957).

Author contributions

Conceptualization and supervision: G.G.Y.; Methodology and investigation: K.L, M.Z.; Visualization: K.L.; Mouse xenograft experiments: M.K. and J.L.; Funding acquisition and project administration: S.J.; Manuscript writing, review, and editing: G.G.Y, D.B.

References

Allard, D., Allard, B. and Stagg, J. (2020). On the mechanism of anti-CD39 immune checkpoint therapy. *J Immunother Cancer* **8**.

Allard, D., Chrobak, P., Allard, B., Messaoudi, N. and Stagg, J. (2018). Targeting the CD73-adenosine axis in immuno-oncology. *Immunology Letters* **205**, 31-9.

Boison, D. (2013). Adenosine kinase: exploitation for therapeutic gain. *Pharmacological Reviews* **65**, 906-943.

Boison, D., Chen, J. F. and Fredholm, B. B. (2010). Adenosine signaling and function in glial cells. *Cell Death Differ* **17**, 1071-82.

Boison, D., Scheurer, L., Zumsteg, V., Rulicke, T., Litynski, P., Fowler, B., Brandner, S. and Mohler, H. (2002). Neonatal hepatic steatosis by disruption of the adenosine kinase gene. *Proc Natl Acad Sci U S A* **99**, 6985-90.

Boison, D. and Yegutkin, G. G. (2019). Adenosine Metabolism: Emerging Concepts for Cancer Therapy. *Cancer Cell* **36**, 582-596.

Borea, P. A., Gessi, S., Merighi, S., Vincenzi, F. and Varani, K. (2018). Pharmacology of Adenosine Receptors: The State of the Art. *Physiological Reviews* **98**, 1591-1625.

Bours, M. J. L., Swennen, E. L. R., Di Virgilio, F., Cronstein, B. N. and Dagnelie, P. C. (2006). Adenosine 5'-triphosphate and adenosine as endogenous signaling molecules in immunity and inflammation. *Pharmacology & Therapeutics* **112**, 358-404.

Bowser, J. L., Lee, J. W., Yuan, X. and Eltzschig, H. K. (2017). The hypoxia-adenosine link during inflammation. *J Appl Physiol (1985)* **123**, 1303-1320.

Carling, D. (2017). AMPK signalling in health and disease. *Current Opinion in Cell Biology* **45**, 31-37.

Casanello, P., Torres, A., Sanhueza, F., Gonzalez, M., Farias, M., Gallardo, V., Pastor-Anglada, M., San Martin, R. and Sobrevia, L. (2005). Equilibrative nucleoside transporter 1 expression is downregulated by hypoxia in human umbilical vein endothelium. *Circulation Research* **97**, 16-24.

Channar, P. A., Afzal, S., Ejaz, S. A., Saeed, A., Larik, F. A., Mahesar, P. A., Lecka, J., Sevigny, J., Erben, M. F. and Iqbal, J. (2018). Exploration of carboxy pyrazole derivatives: Synthesis, alkaline phosphatase, nucleotide pyrophosphatase/phosphodiesterase and nucleoside triphosphate diphosphohydrolase inhibition studies with potential anticancer profile. *Eur J Med Chem* **156**, 461-478.

Chen, H. Y., Chiu, P. Y., Chang, C. J., Tsai, L. L., Huang, Y. L. and Hsu, J. C. (2018). Replacement Effects and Budget Impacts of Insurance Coverage for Sodium-Glucose Co-Transporter-2 Inhibitors on Oral Antidiabetic Drug Utilization. *Clin Drug Investig* **38**, 1125-1133.

Chen, S., Wainwright, D. A., Wu, J. D., Wan, Y., Matei, D. E., Zhang, Y. and Zhang, B. (2019). CD73: an emerging checkpoint for cancer immunotherapy. *Immunotherapy* **11**, 983-997.

Cremers, S., Drake, M. T., Ebetino, F. H., Bilezikian, J. P. and Russell, R. G. G. (2019). Pharmacology of bisphosphonates. *British journal of clinical pharmacology* **85**, 1052-1062.

Di Virgilio, F., Sarti, A. C., Falzoni, S., De Marchi, E. and Adinolfi, E. (2018). Extracellular ATP and P2 purinergic signalling in the tumour microenvironment. *Nat Rev Cancer* **18**, 601-18.

Dzeja, P. P. and Terzic, A. (2003). Phosphotransfer networks and cellular energetics. *Journal of Experimental Biology* **206**, 2039-47.

Eltzschig, H. K., Abdulla, P., Hoffman, E., Hamilton, K. E., Daniels, D., Schonfeld, C., Loffler, M., Reyes, G., Duszenko, M., Karhausen, J. et al. (2005). HIF-1-dependent repression of equilibrative nucleoside transporter (ENT) in hypoxia. *Journal of Experimental Medicine* **202**, 1493-505.

Eltzschig, H. K., Ibla, J. C., Furuta, G. T., Leonard, M. O., Jacobson, K. A., Enjyoji, K., Robson, S. C. and Colgan, S. P. (2003). Coordinated adenine nucleotide phosphohydrolysis and nucleoside signaling in posthypoxic endothelium: role of ectonucleotidases and adenosine A2B receptors. *Journal of Experimental Medicine* **198**, 783-96.

Eltzschig, H. K., Sitkovsky, M. V. and Robson, S. C. (2012). Purinergic signaling during inflammation. *New England Journal of Medicine* **367**, 2322-33.

Hatfield, S. M., Kjaergaard, J., Lukashev, D., Schreiber, T. H., Belikoff, B., Abbott, R., Sethumadhavan, S., Philbrook, P., Ko, K., Cannici, R. et al. (2015). Immunological mechanisms of the antitumor effects of supplemental oxygenation. *Sci Transl Med* **7**, 277ra30.

Helenius, M., Jalkanen, S. and Yegutkin, G. G. (2012). Enzyme-coupled assays for simultaneous detection of nanomolar ATP, ADP, AMP, adenosine, inosine and pyrophosphate concentrations in extracellular fluids. *Biochimica et Biophysica Acta* **1823**, 1967-75.

Horenstein, A. L., Chillemi, A., Zaccarello, G., Bruzzone, S., Quarona, V., Zito, A., Serra, S. and Malavasi, F. (2013). A CD38/CD203a/CD73 ectoenzymatic pathway independent of CD39 drives a novel adenosinergic loop in human T lymphocytes. *Oncoimmunology* **2**, e26246.

Jacobson, K. A. and Muller, C. E. (2016). Medicinal chemistry of adenosine, P2Y and P2X receptors. *Neuropharmacology* **104**, 31-49.

Janes, P. W., Ley, S. C. and Magee, A. I. (1999). Aggregation of lipid rafts accompanies signaling via the T cell antigen receptor. *Journal of Cell Biology* **147**, 447-61.

Kobayashi, S., Zimmermann, H. and Millhorn, D. E. (2000). Chronic hypoxia enhances adenosine release in rat PC12 cells by altering adenosine metabolism and membrane transport. *J Neurochem* **74**, 621-32.

Krys, D., Hamann, I., Wuest, M. and Wuest, F. (2019). Effect of hypoxia on human equilibrative nucleoside transporters hENT1 and hENT2 in breast cancer. *The FASEB Journal* **33**, 13837–13851.

Lau, W. M., Doucet, M., Stadel, R., Huang, D., Weber, K. L. and Kominsky, S. L. (2013). Enpp1: a potential facilitator of breast cancer bone metastasis. *PLoS One* **8**, e66752.

Ledoux, S., Runembert, I., Koumanov, K., Michel, J. B., Trugnan, G. and Friedlander, G. (2003). Hypoxia enhances Ecto-5'-Nucleotidase activity and cell surface expression in endothelial cells: role of membrane lipids. *Circulation Research* **92**, 848-55.

Lee, P., Chandel, N. S. and Simon, M. C. (2020). Cellular adaptation to hypoxia through hypoxia inducible factors and beyond. *Nat Rev Mol Cell Biol*.

Lee, S. Y. and Muller, C. E. (2017). Nucleotide pyrophosphatase/phosphodiesterase 1 (NPP1) and its inhibitors. *Medchemcomm* **8**, 823-840.

Li, X. Y., Moesta, A. K., Xiao, C., Nakamura, K., Casey, M., Zhang, H., Madore, J., Lepletier, A., Roman Aguilera, A., Sundarrajan, A. et al. (2019). Targeting CD39 in cancer reveals an extracellular ATP and inflammasome driven tumor immunity. *Cancer Discov*, 1754-1773.

Losenkova, K., Paul, M., Irjala, H., Jalkanen, S. and Yegutkin, G. G. (2020). Histochemical Approach for Simultaneous Detection of Ectonucleotidase and Alkaline Phosphatase Activities in Tissues. *Methods Mol Biol* **2041**, 107-116.

Losenkova, K., Zuccarini, M., Helenius, M., Jacquemet, G., Gerasimovskaya, E., Tallgren, C., Jalkanen, S. and Yegutkin, G. G. (2018). Endothelial cells cope with hypoxia-induced depletion of ATP via activation of cellular purine turnover and phosphotransfer networks. *Biochimica et Biophysica Acta* **1864**, 1804-1815.

Maj, T., Wang, W., Crespo, J., Zhang, H., Wei, S., Zhao, L., Vatan, L., Shao, I., Szeliga, W., Lyssiotis, C. et al. (2017). Oxidative stress controls regulatory T cell apoptosis and suppressor activity and PD-L1-blockade resistance in tumor. *Nat Immunol* **18**, 1332-1341.

Martinez-Outschoorn, U. E., Peiris-Pages, M., Pestell, R. G., Sotgia, F. and Lisanti, M. P. (2017). Cancer metabolism: a therapeutic perspective. *Nat Rev Clin Oncol* **14**, 11-31.

Mercier, N., Kiviniemi, T. O., Saraste, A., Miiluniemi, M., Silvola, J., Jalkanen, S. and Yegutkin, G. G. (2012). Impaired ATP-Induced Coronary Blood Flow and Diminished Aortic NTPDase Activity Precede Lesion Formation in Apolipoprotein E-Deficient Mice. *American Journal of Pathology* **180**, 419-28.

Ohta, A., Gorelik, E., Prasad, S. J., Ronchese, F., Lukashev, D., Wong, M. K., Huang, X., Caldwell, S., Liu, K., Smith, P. et al. (2006). A2A adenosine receptor protects tumors from antitumor T cells. *Proc Natl Acad Sci U S A* **103**, 13132-7.

Orriss, I. R., Arnett, T. R. and Russell, R. G. (2016). Pyrophosphate: a key inhibitor of mineralisation. *Curr Opin Pharmacol* **28**, 57-68.

Pignataro, G., Maysami, S., Studer, F. E., Wilz, A., Simon, R. P. and Boison, D. (2008). Downregulation of hippocampal adenosine kinase after focal ischemia as potential endogenous neuroprotective mechanism. *Journal of Cerebral Blood Flow and Metabolism* **28**, 17-23.

Rasool, R. U., Nayak, D., Chakraborty, S., Jamwal, V. L., Mahajan, V., Katoch, A., Faheem, M. M., Iqra, Z., Amin, H., Gandhi, S. G. et al. (2017). Differential regulation of NM23-H1 under hypoxic and serum starvation conditions in metastatic cancer cells and its implication in EMT. *European Journal of Cell Biology* **96**, 164-171.

Roberts, F., Zhu, D., Farquharson, C. and Macrae, V. E. (2019). ENPP1 in the Regulation of Mineralization and Beyond. *Trends in Biochemical Sciences* **44**, 616-628.

Robson, S. C., Wu, Y., Sun, X., Knosalla, C., Dwyer, K. and Enjyoji, K. (2005). Ectonucleotidases of CD39 family modulate vascular inflammation and thrombosis in transplantation. *Semin Thromb Hemost* **31**, 217-33.

Romani, P., Ignesti, M., Gargiulo, G., Hsu, T. and Cavaliere, V. (2018). Extracellular NME proteins: a player or a bystander? *Laboratory Investigation* **98**, 248-257.

Roy, C., Tabiasco, J., Caillon, A., Delneste, Y., Merot, J., Favre, J., Guihot, A. L., Martin, L., Nascimento, D. C., Ryffel, B. et al. (2018). Loss of vascular expression of nucleoside triphosphate diphosphohydrolase-1/CD39 in hypertension. *Purinergic Signal* **14**, 73-82.

Schiedel, A. C., Lacher, S. K., Linnemann, C., Knolle, P. A. and Muller, C. E. (2013). Antiproliferative effects of selective adenosine receptor agonists and antagonists on human lymphocytes: evidence for receptor-independent mechanisms. *Purinergic Signal* **9**, 351-65.

Schneider, C. A., Rasband, W. S. and Eliceiri, K. W. (2012). NIH Image to ImageJ: 25 years of image analysis. *Nat Methods* **9**, 671-5.

Sitkovsky, M. V., Hatfield, S., Abbott, R., Belikoff, B., Lukashev, D. and Ohta, A. (2014). Hostile, hypoxia-A2-adenosinergic tumor biology as the next barrier to overcome for tumor immunologists. *Cancer Immunol Res* **2**, 598-605.

Spychala, J. (2000). Tumor-promoting functions of adenosine. *Pharmacology and Therapeutics* **87**, 161-73.

Synnestvedt, K., Furuta, G. T., Comerford, K. M., Louis, N., Karhausen, J., Eltzschig, H. K., Hansen, K. R., Thompson, L. F. and Colgan, S. P. (2002). Ecto-5'-nucleotidase (CD73) regulation by hypoxia-inducible factor-1 mediates permeability changes in intestinal epithelia. *Journal of Clinical Investigation* **110**, 993-1002.

Toti, K. S., Osborne, D., Ciancetta, A., Boison, D. and Jacobson, K. A. (2016). South (S)- and North (N)-Methanocarba-7-Deazaadenosine Analogues as Inhibitors of Human Adenosine Kinase. *Journal of Medicinal Chemistry* **59**, 6860-77.

Turner, M. S., Haywood, G. A., Andreka, P., You, L., Martin, P. E., Evans, W. H., Webster, K. A. and Bishopric, N. H. (2004). Reversible connexin 43 dephosphorylation during hypoxia and reoxygenation is linked to cellular ATP levels. *Circulation Research* **95**, 726-33.

Vaupel, P. and Multhoff, G. (2017). Accomplices of the Hypoxic Tumor Microenvironment Compromising Antitumor Immunity: Adenosine, Lactate, Acidosis, Vascular Endothelial Growth Factor, Potassium Ions, and Phosphatidylserine. *Front Immunol* **8**, 1887.

Vijayan, D., Young, A., Teng, M. W. L. and Smyth, M. J. (2017). Targeting immunosuppressive adenosine in cancer. *Nat Rev Cancer* **17**, 709-724.

Virtanen, S. S., Kukkonen-Macchi, A., Vainio, M., Elima, K., Harkonen, P. L., Jalkanen, S. and Yegutkin, G. G. (2014). Adenosine Inhibits Tumor Cell Invasion via Receptor-Independent Mechanisms. *Mol Cancer Res* **12**, 1863-74.

Visovatti, S. H., Hyman, M. C., Goonewardena, S. N., Anyanwu, A. C., Kanthi, Y., Robichaud, P., Wang, J., Petrovic-Djergovic, D., Rattan, R., Burant, C. F. et al. (2016). Purinergic dysregulation in pulmonary hypertension. *Am J Physiol Heart Circ Physiol* **311**, H286-98.

Williams-Karnesky, R. L., Sandau, U. S., Lusardi, T. A., Lytle, N. K., Farrell, J. M., Pritchard, E. M., Kaplan, D. L. and Boison, D. (2013). Epigenetic changes induced by adenosine augmentation therapy prevent epileptogenesis. *Journal of Clinical Investigation* **123**, 3552-63.

Xu, Y., Wang, Y., Yan, S., Yang, Q., Zhou, Y., Zeng, X., Liu, Z., An, X., Toque, H. A., Dong, Z. et al. (2017). Regulation of endothelial intracellular adenosine via adenosine kinase epigenetically modulates vascular inflammation. *Nat Commun* **8**, 943.

Xu, Z., Singh, N. J., Lim, J., Pan, J., Kim, H. N., Park, S., Kim, K. S. and Yoon, J. (2009). Unique sandwich stacking of pyrene-adenine-pyrene for selective and ratiometric fluorescent sensing of ATP at physiological pH. *J Am Chem Soc* **131**, 15528-33.

Yegutkin, G. G. (2008). Nucleotide- and nucleoside-converting ectoenzymes: Important modulators of purinergic signalling cascade. *Biochimica et Biophysica Acta* **1783**, 673-94.

Yegutkin, G. G. (2014). Enzymes involved in metabolism of extracellular nucleotides and nucleosides: Functional implications and measurement of activities. *Crit Rev Biochem Mol Biol* **49**, 473-97.

Yegutkin, G. G., Helenius, M., Kaczmarek, E., Burns, N., Jalkanen, S., Stenmark, K. and Gerasimovskaya, E. V. (2011). Chronic hypoxia impairs extracellular nucleotide metabolism and barrier function in pulmonary artery vasa vasorum endothelial cells. *Angiogenesis* **14**, 503-13.

Yegutkin, G. G., Henttinen, T. and Jalkanen, S. (2001). Extracellular ATP formation on vascular endothelial cells is mediated by ecto-nucleotide kinase activities via phosphotransfer reactions. *Faseb Journal* **15**, 251-260.

Yegutkin, G. G., Mikhailov, A., Samburski, S. S. and Jalkanen, S. (2006). The detection of micromolar pericellular ATP pool on lymphocyte surface by using lymphoid ecto-adenylate kinase as intrinsic ATP sensor. *Molecular Biology of the Cell* **17**, 3378-85.

Yokdang, N., Nordmeier, S., Speirs, K., Burkin, H. R. and Buxton, I. L. (2015). Blockade of extracellular NM23 or its endothelial target slows breast cancer growth and metastasis. *Integr Cancer Sci Ther* **2**, 192-200.

Zimmermann, H., Zebisch, M. and Strater, N. (2012). Cellular function and molecular structure of ecto-nucleotidases. *Purinergic Signal* **8**, 437-502.

Figures

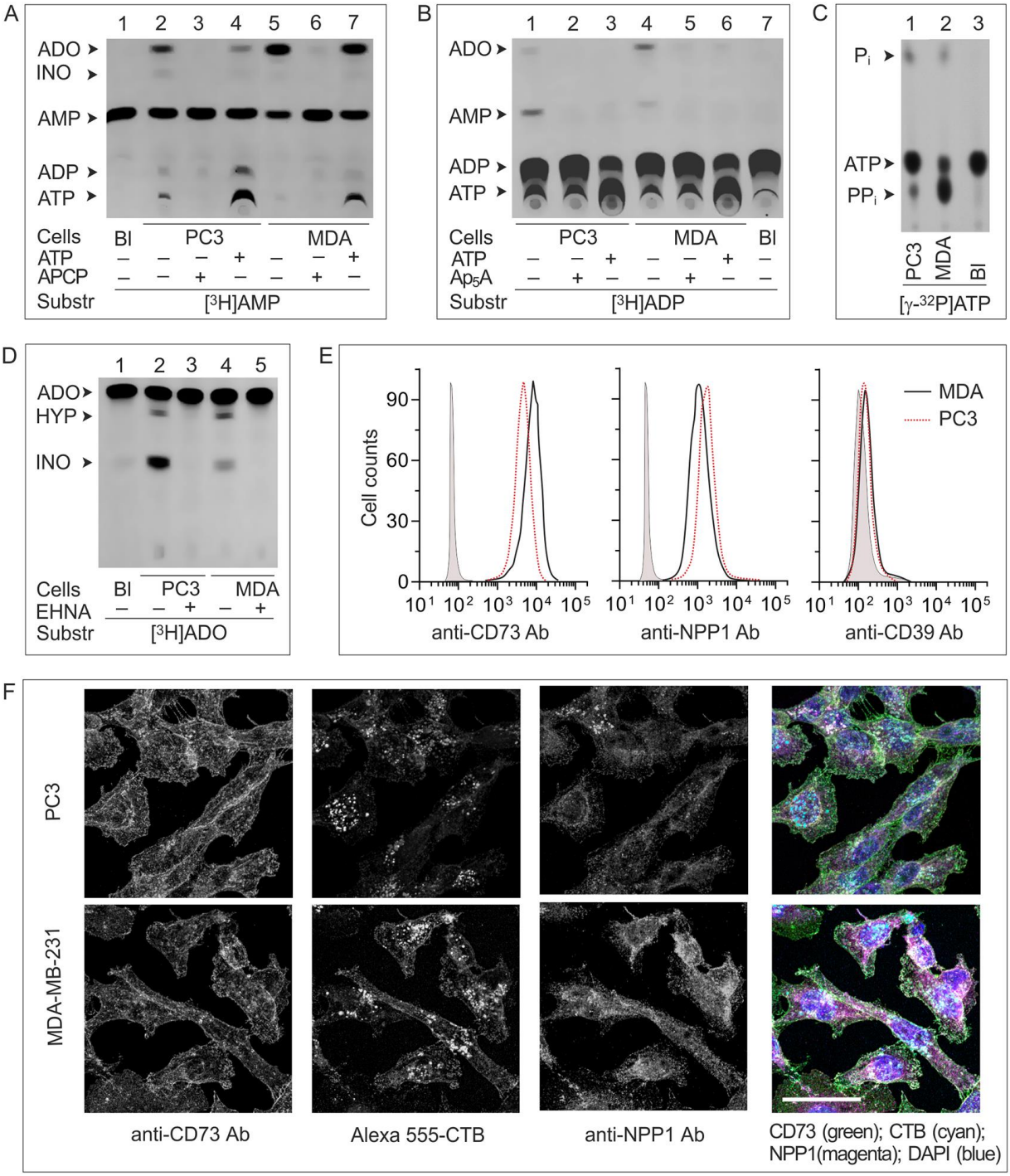

Fig. 1. Characterization of extracellular purine-converting pathways in the human cancer cells. PC3 and MDA-MB-231 (*MDA*) cells were incubated with 100 μM [^{3}H]AMP (A), 20 μM [^{3}H]ADP (B), 10 μM [γ-^{32}P]ATP (C), and 50 μM [^{3}H]ADO (D). In some competitive assays, the cells were pre-treated with ATP (300 μM), APCP (100 μM), Ap_5A (100 μM) or EHNA (10 μM), as indicated. Aliquots of the mixtures were separated by TLC using appropriate solvent systems and developed by autoradiography. The blanks (Bl) show the radiochemical purities of ^{3}H- and ^{32}P-labeled substrates in the absence of cells. Arrows indicate the position of nucleotide standards, adenosine (*ADO*), inosine (*INO*), hypoxanthine (*HYP*),

inorganic phosphate (P_i) and pyrophosphate (PP_i). (E) The expression levels of ecto-nucleotidases were assayed by flow cytometry, using antibodies against CD73 (4G4), NPP1 (CD203a), and CD39 (hN1-1_C), as well as isotype-matched control immunoglobulins (shown in gray). (F) Cell surface expression of NPP1 and CD73 was independently validated using confocal microscopy by co-staining PC3 and MDA-MB-231 cells with anti-CD73 (h5NT-1_L) and anti-NPP1 (CD203a) antibodies, together with Alexa Fluor® 555-conjugated cholera toxin subunit-B (CTB). Scale bar, 40 µm.

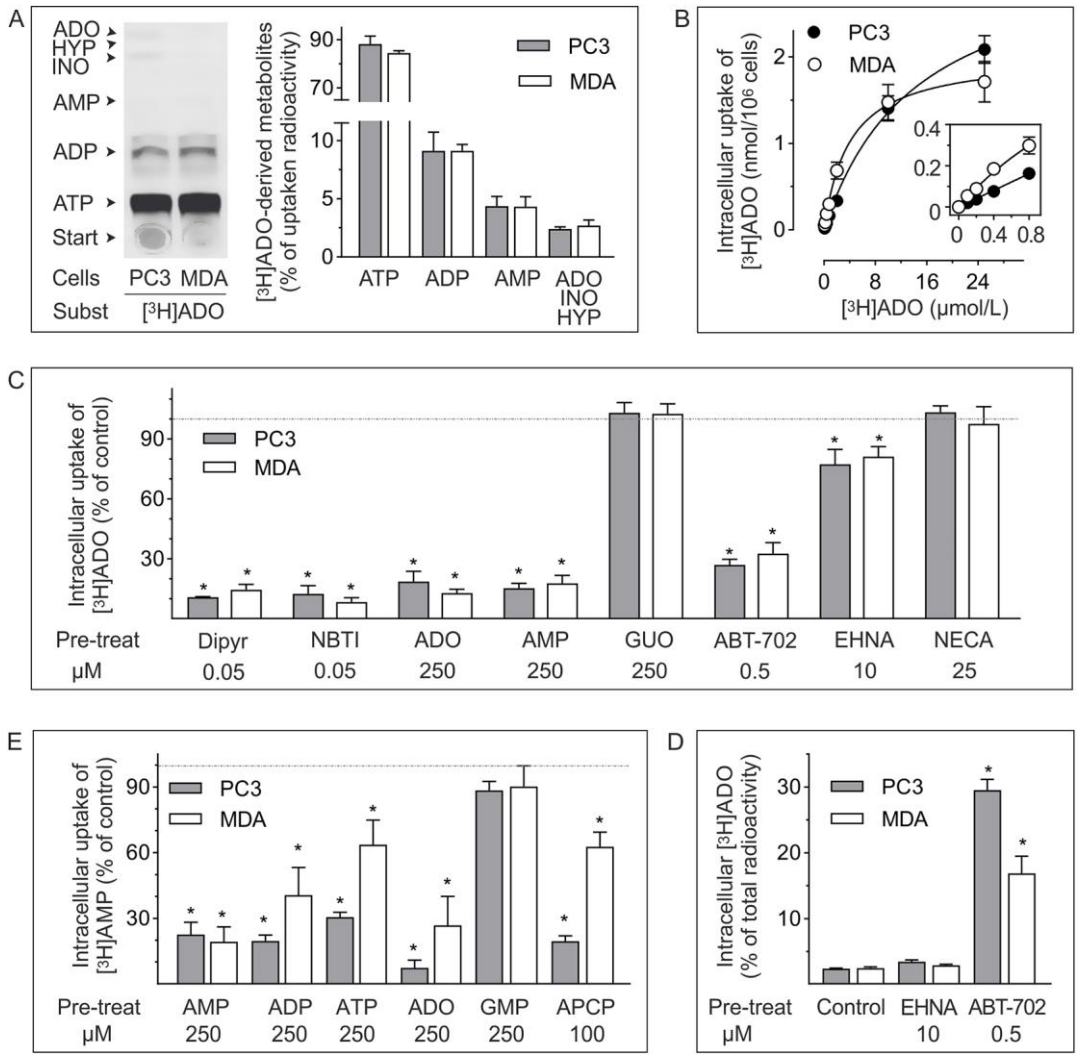

Fig. 2. Intracellular ADO uptake and metabolism by the human cancer cells. (A) PC3 and MDA-MB-231 (*MDA*) cells were incubated for 45 min with 10 μM [^{3}H]ADO, lysed, separated by TLC and subsequently analyzed for ^{3}H-metabolites using autoradiographic imaging or scintillation β-counting. Right panel shows the relative amounts of intracellularly formed ATP, ADP, AMP and nucleosides (determined as pooled ADO, INO and HYP fractions) (mean ± SEM; n=5). (B) Kinetic analysis of cellular ADO uptake was performed by incubating the cells with [^{3}H]ADO and the increasing concentrations of unlabeled ADO. Fitting the constructed concentration-response curves to a one-site model determined a limited capability of PC3 and MDA-MB-231 cells to uptake ADO, with maximum loading capacity (B_{max}) equal to 3.3 ± 0.4 (mean ± SEM; n=3) and 2.0 ± 0.2 (n=6) nmol/10^6 cells, respectively. The cells were also pre-treated with the indicated concentrations of nucleotide and nucleoside analogues and subsequently incubated with 10 μM [^{3}H]ADO (C) or 10 μM [^{3}H]AMP (D). The results are expressed as a percentage of total cell-incorporated radioactivity determined in control, vehicle-treated, cells (mean ± SEM; n=3-6). (E) The relative amounts of intracellular [^{3}H]ADO were determined in PC3 and MDA-MB-231 cells incubated for 60 min without (Control) and with 10 μM EHNA or 500 nM ABT-702 prior to addition of 200 nM [^{3}H]ADO (mean ± SEM; n=4-5). *P<0.05.

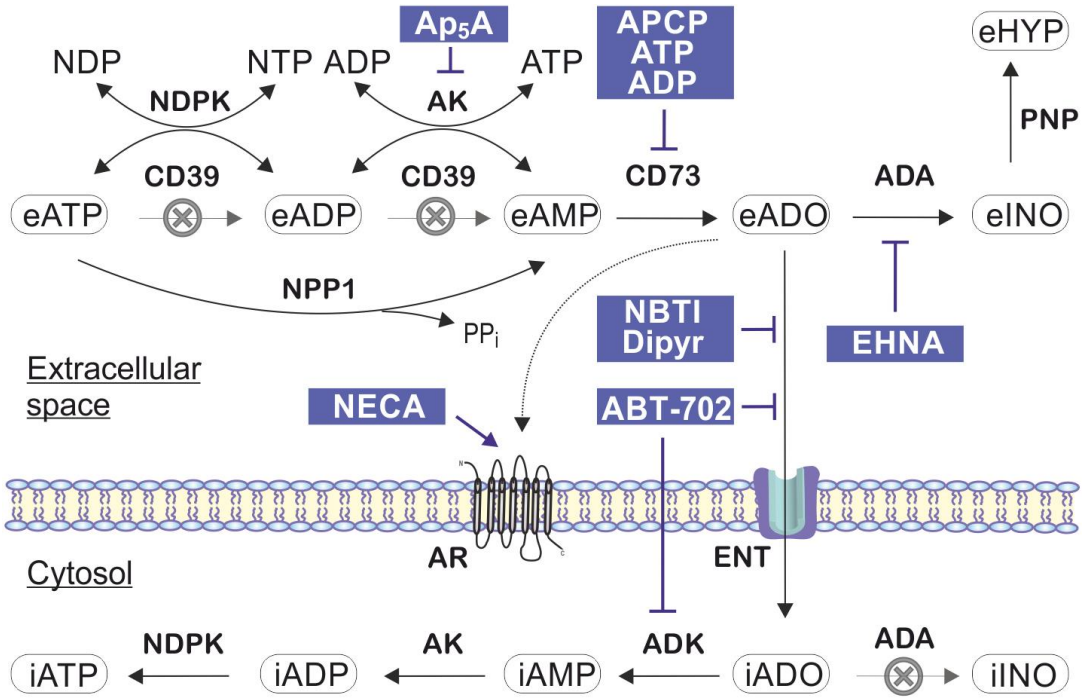

Fig. 3. Compartmentalization of adenosine biochemistry in cancer cells. Cellular purine turnover is comprised of (i) the release of endogenous ATP and its binding to nucleotide-selective P2X and P2Y receptors (not shown); (ii) the metabolism of extracellular ATP (eATP) and other nucleotides and nucleosides via concerted action of purine-inactivating and ATP-regenerating ectoenzymes; (iii) triggering of signaling events via adenosine receptors (AR); (iv) the uptake of nucleotide-derived eADO via equilibrative nucleoside transporters (ENT) and its sequential phosphorylation into intracellular ATP (iATP). General schemes of adenosine producing and removing pathways in the epithelial-derived carcinoma cells have included a role for the enzymes nucleotide pyrophosphatase/phosphodiesterase-1 (NPP1), ecto-5'-nucleotidase/CD73 and adenosine deaminase (ADA), while NTPDase1/CD39 do not seem to contribute significantly to the metabolism of nucleotides. In addition, counteracting adenylate kinase (AK) and nucleotide diphosphokinase (NDPK) contribute to the active cycling between extracellular ATP and ADP. The generated ATP and AMP are then metabolized through the coupled NPP1 and CD73 reactions, respectively. Intracellular adenosine metabolism mainly depends on spatially arranged phosphotransfer networks, catalyzed by cytosolic isoforms of adenosine kinase (ADK), AK, and NDPK. Sites of directional inhibition of these metabolic pathways by selective inhibitors and activation of adenosinergic signaling by non-selective AR agonist NECA are pointed by blunted and open bold blue arrows, respectively. For the sake of clarity only the most important enzymes are mentioned.

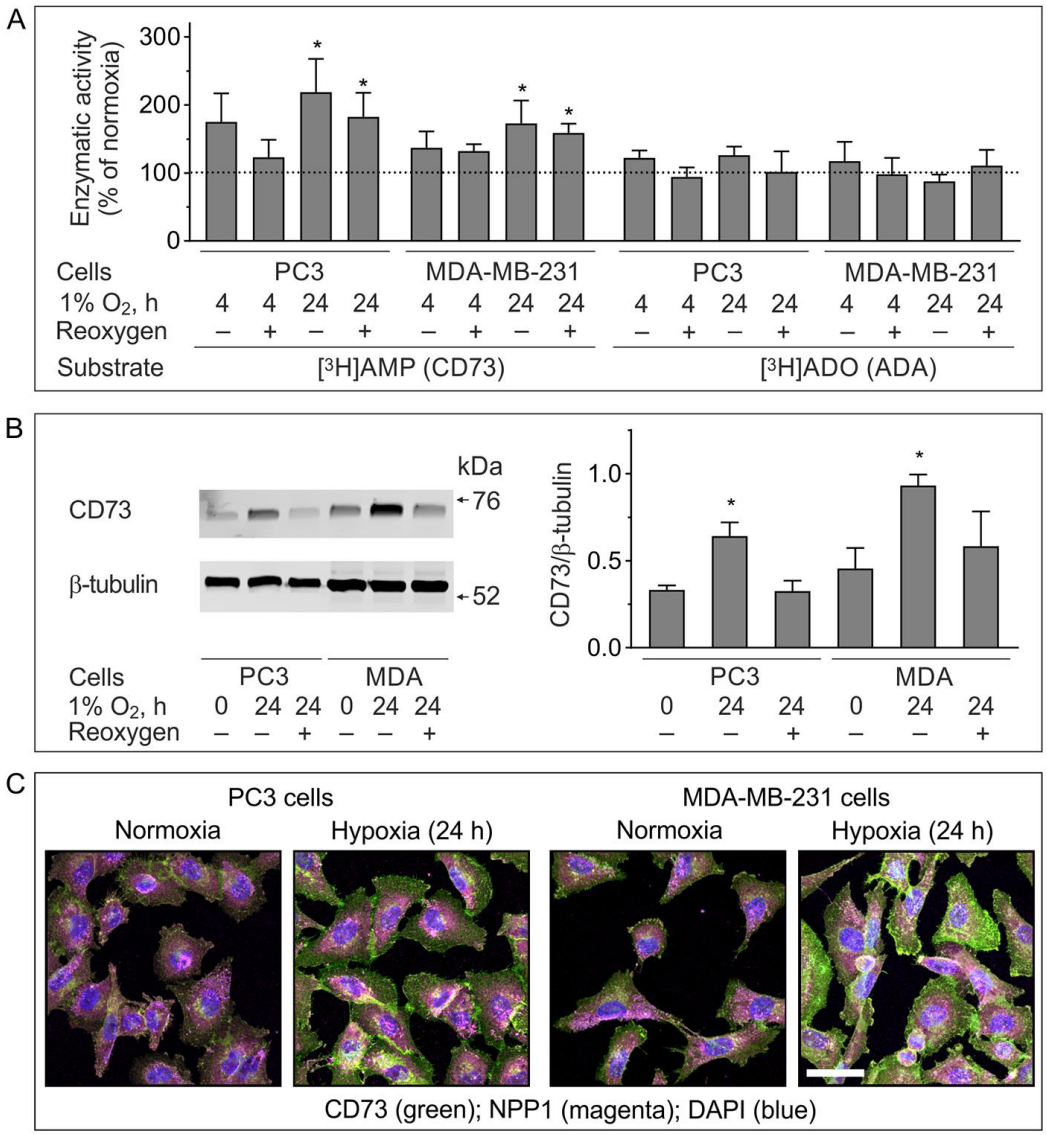

Fig. 4. The effect of hypoxia on extracellular purine metabolism. PC3 and MDA-MB-231 (*MDA*) cells were exposed to hypoxia (0-24 hours) with or without a subsequent 1-hour re-oxygenation. (A) The treated cells were assayed for ecto-5'-nucleotidase/CD73 (*CD73*) and adenosine deaminase (*ADA*) activities using 300 μM [^{3}H]AMP and [^{3}H]ADO, as respective enzyme substrates. The results are expressed as a percentage of AMP-hydrolyzing and adenosine-deaminating activities determined in normoxic cells (mean ± SEM, n=4-8). (B) Western blot analysis of PC3 and MDA-MB-231 cell lysates stained with anti-CD73 antibody (D7F9A) and anti-β-tubulin mAb (TUB2.1) as a control for protein loading. The arrows indicate the positions of the molecular mass markers (kDa). Mean intensities of the bands were quantified using ImageJ and expressed as CD73-to-β-tubulin ratio (mean ± SEM, n=3). *P<0.05 as compared with control normoxic cells. (C) MDA-MB-231 and PC3 cells grown on coverslips were subjected to hypoxia for 24 hours and processed for co-staining with anti-CD73 (h5NT-1$_L$) and anti-NPP1 (CD203a) antibodies. The panels show the merged images with nuclei counterstained with blue-fluorescent DAPI. For single channel view, see Supplementary Fig. S1. Scale bar, 50 μm.

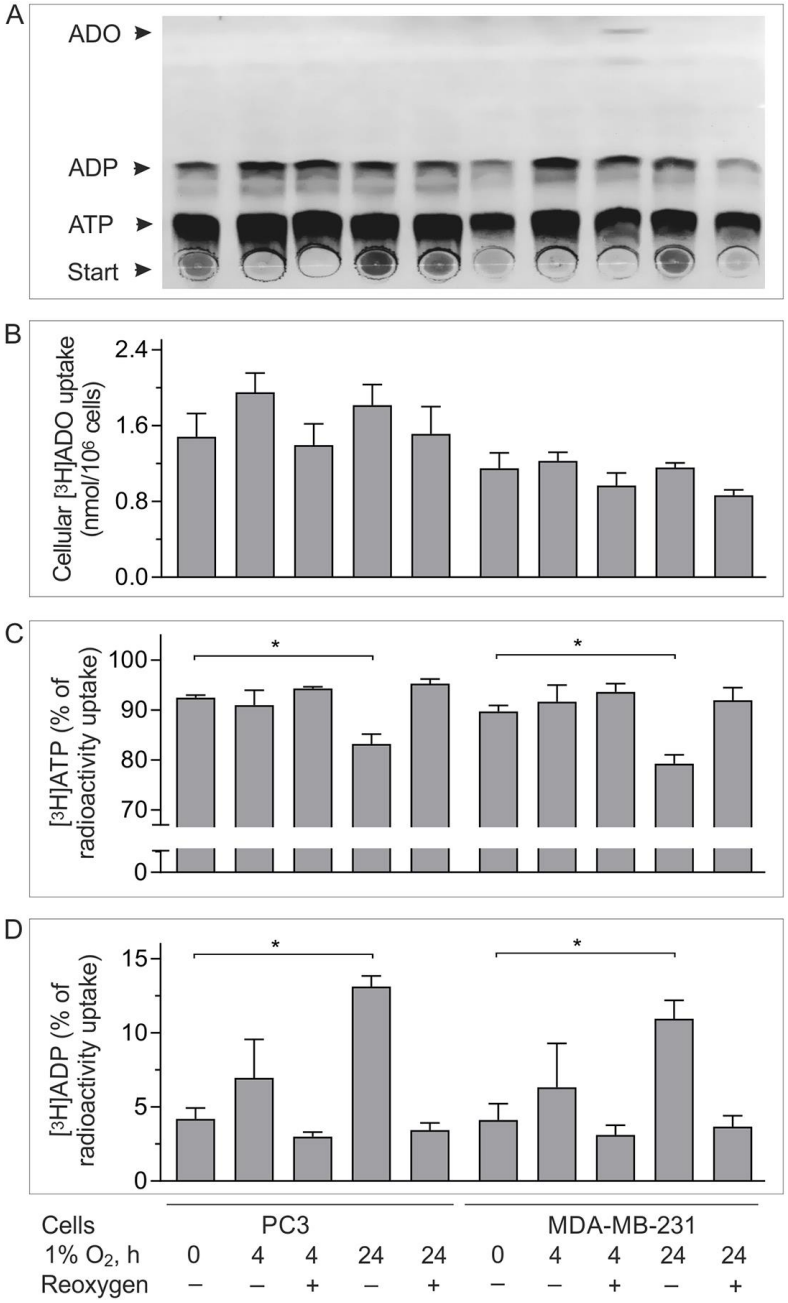

Fig. 5. Cellular [^{3}H]ADO uptake and metabolism in normoxic and hypoxic cancer cells. Cultured PC3 and MDA-MB-231 cells were subjected to acute hypoxia (4-24 hours) with or without subsequent 1-hour reoxygenation. The treated cells were incubated then with 10 μM [^{3}H]ADO, washed, lysed and separated by TLC. Panel A depicts a representative autoradiographic image of an overall pattern of intracellular metabolism of ^{3}H-purines in normoxic and hypoxic cells. Arrows indicate the positions of nucleotide and ADO standards. (B) Total amount of cell-incorporated radioactivity was determined and expressed as nanomoles of [^{3}H]ADO taken up by 10^6 cells (mean ± SEM, n=4). *P<0.05. The conversion of [^{3}H]ADO into its phosphorylated metabolites, [^{3}H]ATP (C) and [^{3}H]ADP (D), was quantified by scintillation β-counting and expressed as percentage of total cell-incorporated radioactivity (mean ± SEM, n=3-5).

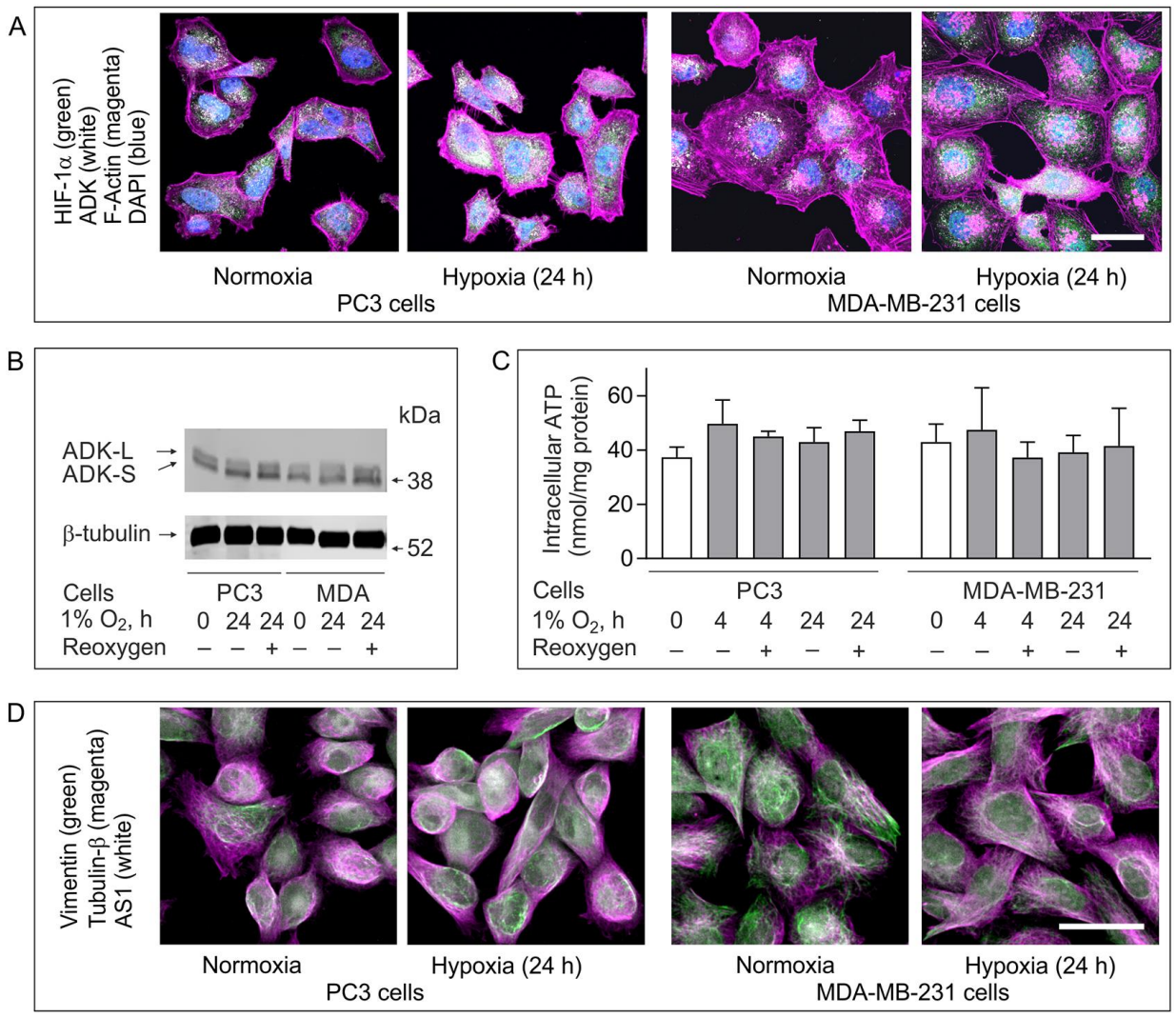

Fig. 6. Characterization of cellular ATP, HIF-1α and ADK levels in normoxic and hypoxic cancer cells. PC3 and MDA-MB-231 (*MDA*) cells grown on coverslips were subjected to 24-hour hypoxia with or without subsequent 1-hour reoxygenation. (A) The treated cells were fixed, permeabilized, and co-stained with the antibodies against HIF-1α and ADK, together with Alexa Fluor® 546-conjugated Phalloidin. The panels show the merged images counterstained with DAPI. (B) The expression levels of cytosolic (ADK-S) and nuclear (ADK-L) isoforms of ADK were determined in the cell lysates, by using Western blot analysis. For each experiment, the blots were probed with an anti-β-tubulin mAb to normalize for protein loading. The arrows indicate the positions of the molecular mass markers (kDa). Mean intensities of the bands were quantified using ImageJ and summarized in Supplementary Fig. S3. (C) Cellular ATP content was determined in the cell lysates by using a bioluminescent luciferin-luciferase assay and expressed as nanomoles of ATP per mg protein (mean ± SEM; n=4-6). (D) Normoxic and hypoxic cells were co-stained with a fluorescent ATP-sensing dye, AS1, in combination with anti-vimentin and anti-β-tubulin antibodies. For single channel view, see Supplementary Figures S2 and S5. Scale bars, 40 µm.

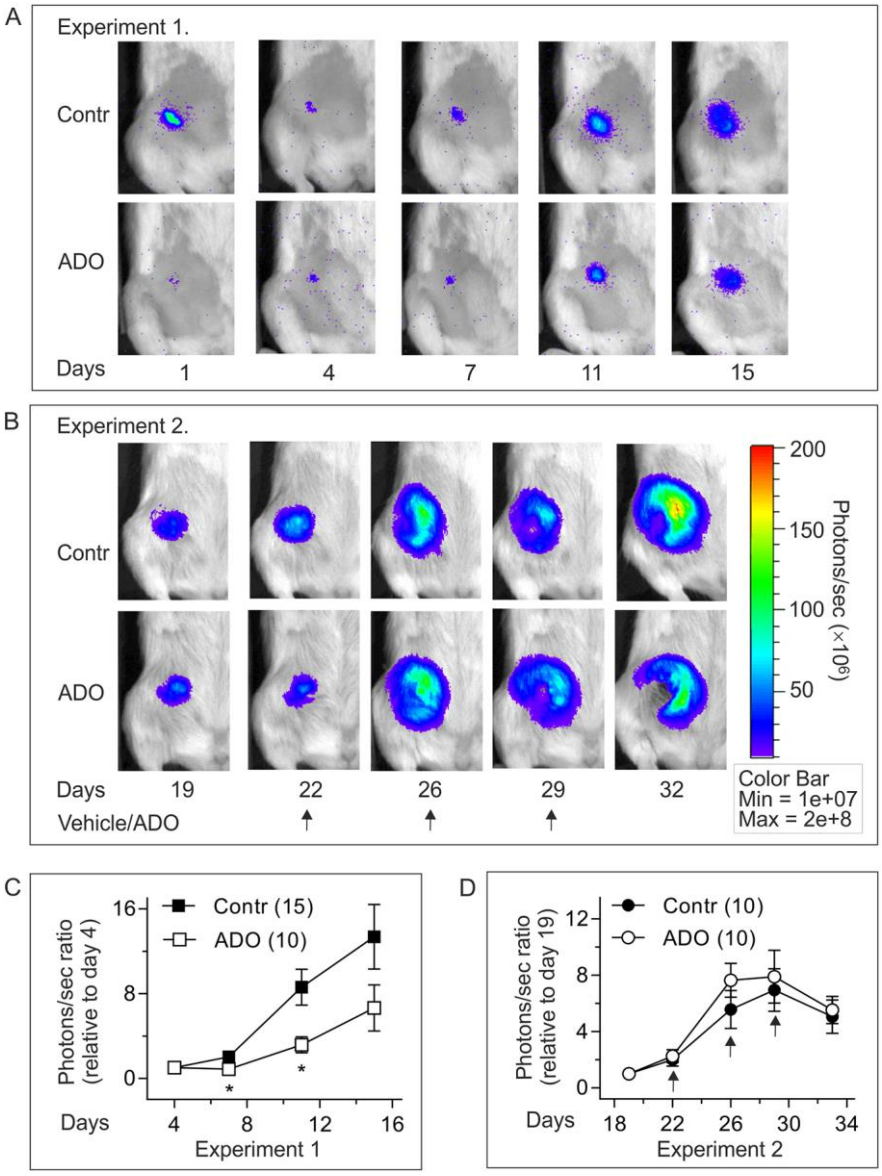

Fig. 7. Effect of ADO on tumor growth in xenograft breast cancer model. (A) Human MDA-MB-231-luc-D3H2LN cells were pre-treated without (*Contr*) and with 100 μM ADO, and subsequently inoculated into the mammary fat pads of female SCID mice on day 0. The panels display representative images of mice in dorsal positions scanned on days 1, 4, 7, 11, and 15 to monitor the growth of vehicle- and ADO-treated tumors. (B) In the second experiments, the established primary mammary tumors were periodically treated with 50 μl of ADO (100 μM) or equal volumes of PBS. The panels show bioluminescence signals over time for representative individual tumors, with intratumoral treatments pointed out by arrows. All images show photon flux from bioluminescence on a pseudocolor scale, with red and blue representing the highest and lowest values, respectively. Panels C and D summarize the data from the first and second experiments, which were quantified, corrected for background signal, and normalized relative to day 4 and 19, respectively. The numbers of animals in each group are shown in parentheses. *P<0.05, determined by multiple t-test grouped analysis.

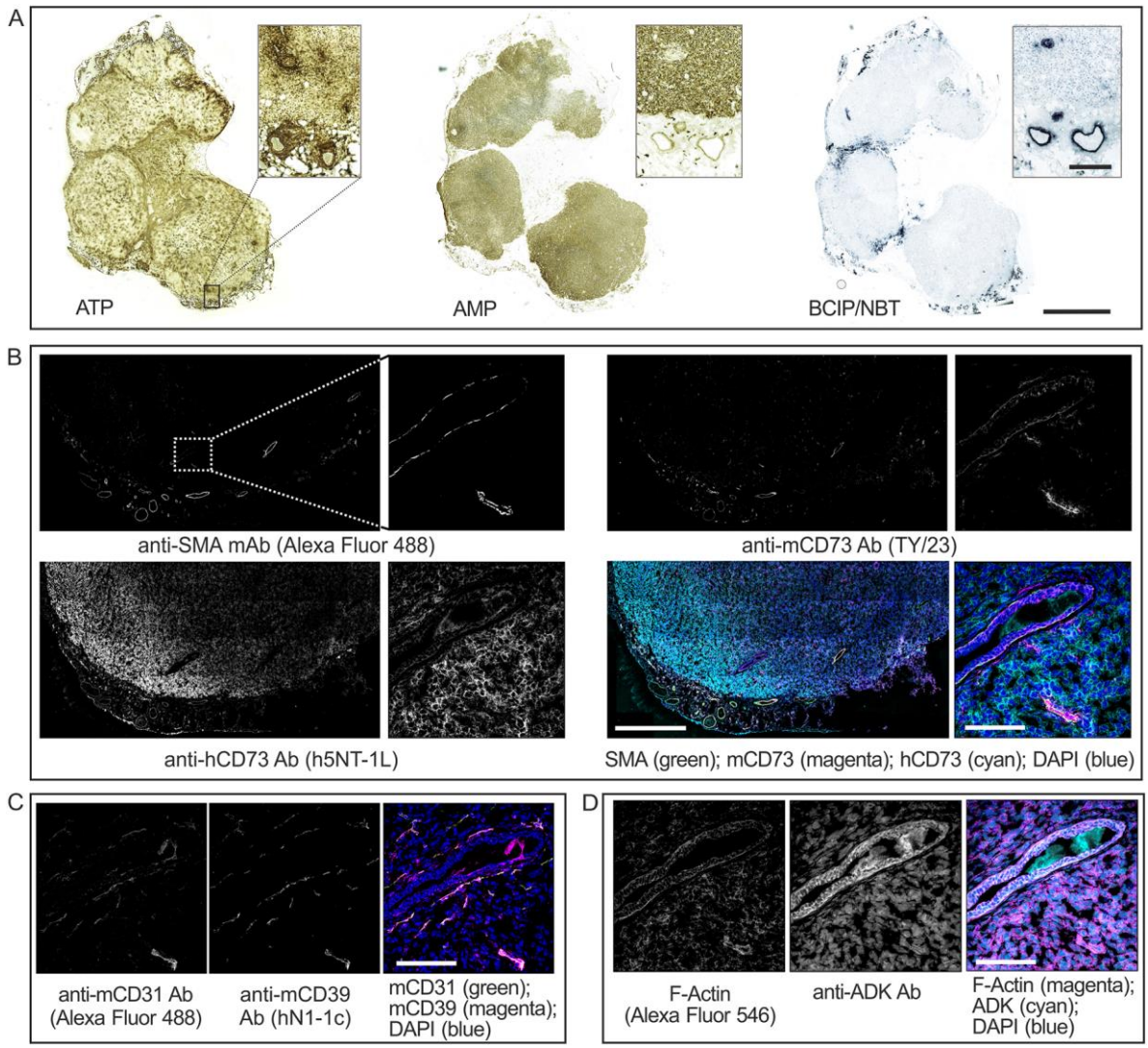

Fig. 8. Distribution of purine-converting enzymes in the breast cancer xenograft. (A) Tumor ecto-nucleotidases were assayed by incubating tissue cryosections with 400 μM ATP or AMP in the presence of $Pb(NO_4)_2$, followed by microscopic detection of nucleotide-derived P_i as a brown precipitate. The activity of TNAP was measured by using the artificial chromogenic enzyme substrate BCIP/NBT (400 μM each) and subsequent monitoring the development of blue staining. For immunofluorescence staining, tumor slices were incubated with rat anti-mouse and rabbit anti-human CD73 antibodies (B), guinea pig anti-mouse CD39 antibody (C), and rabbit anti-ADK antibody (D), and subsequently stained with isotype-matched fluorochrome-conjugated secondary antibodies, in combination with selective markers of smooth muscle cells (Alexa Fluor® 488-SMA), F-actin (Alexa Fluor® 546-Phalloidin), and vascular endothelium (Alexa Fluor® 488-CD31), as indicated. Nuclei were counterstained with blue-fluorescent DAPI. Scale bars, 3 mm (A), 250 μm (A, inset), 1 mm (B, left), and 100 μm (B, right panels, C, and D).

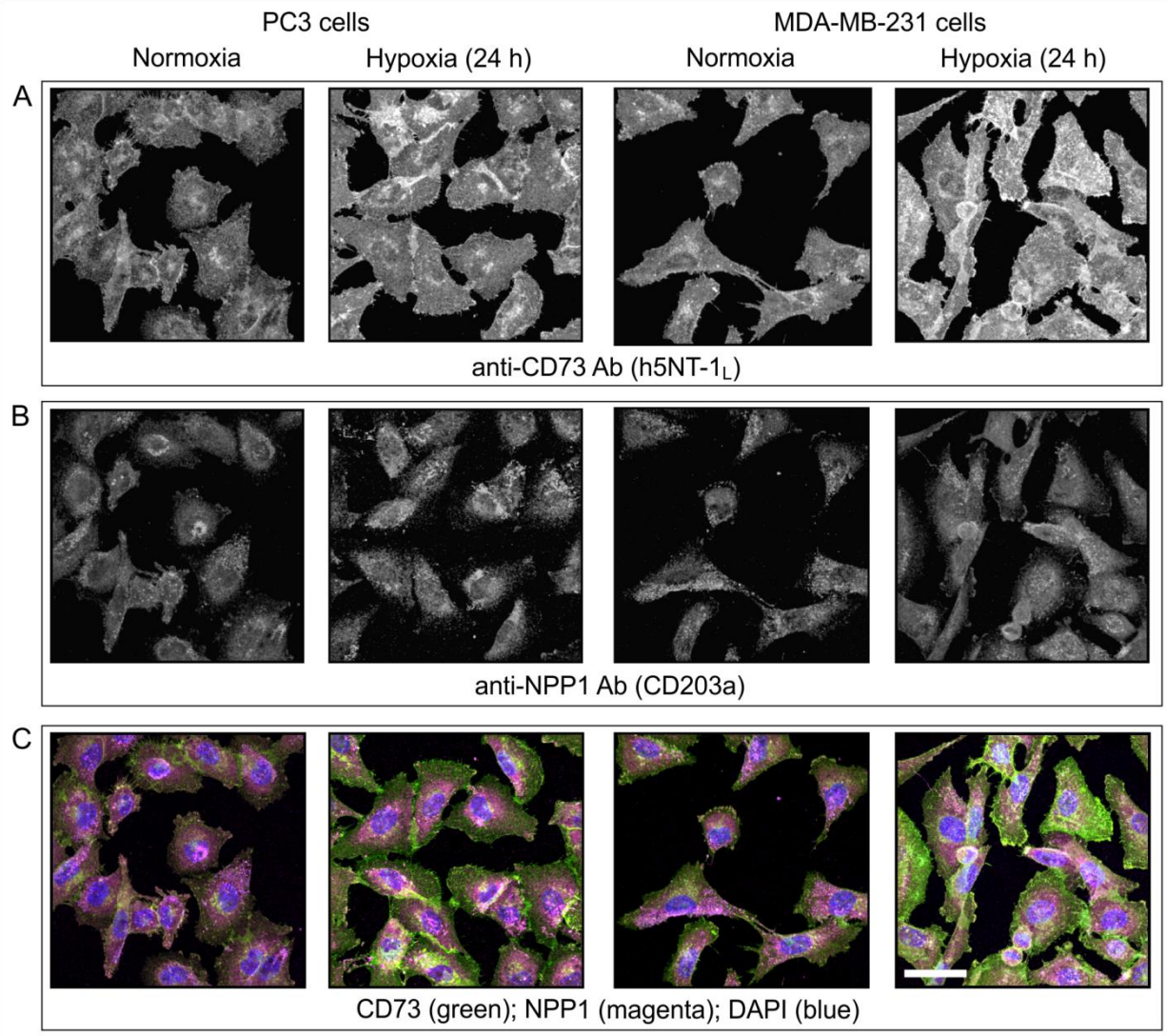

Fig. S1. The effect of hypoxia on extracellular expression of CD73 and NPP1. MDA-MB-231 and PC3 cells grown on coverslips were incubated for 24 hours in the incubator with 21% O_2 (*"Normoxia"*) or in the hypoxic chamber containing 1% O_2 ("*Hypoxia*"). The treated cells were processed for co-staining with anti-CD73 (A) and anti-NPP1 (B) antibodies. The panel C shows the merged images with nuclei counterstained with blue-fluorescent DAPI. Scale bar, 50 µm.

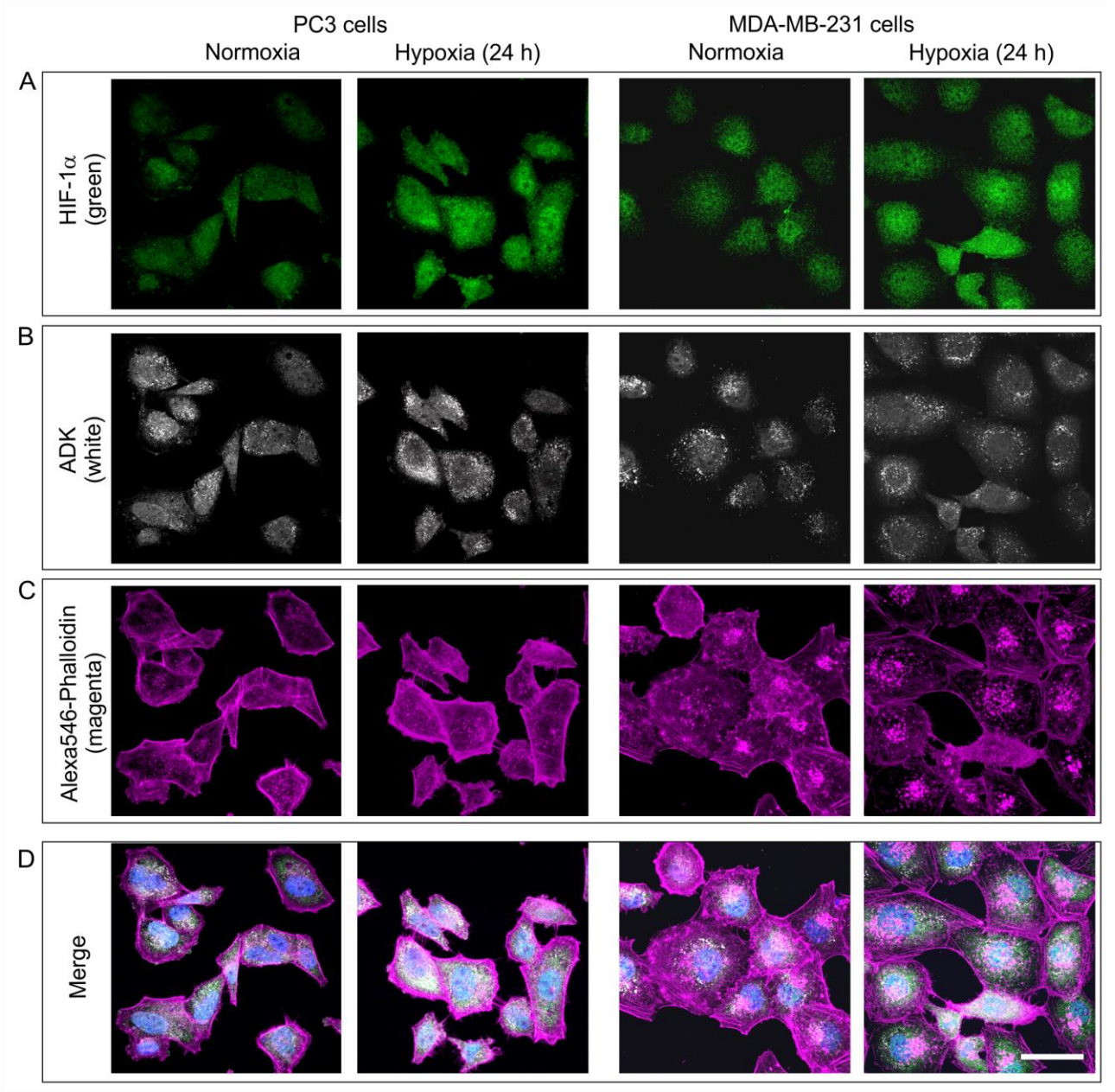

Fig. S2. The effect of hypoxia on cellular expression of HIF-1α and ADK. PC3 and MDA-MB-231 cells grown on coverslips were incubated for 24 hours in the incubator with 21% O_2 (*"Normoxia"*) or in the hypoxic chamber containing 1% O_2 ("*Hypoxia*"). The treated cells were fixed, permeabilized, and co-stained with the antibodies against HIF-1α (A) and ADK (B), together with Alexa Fluor® 546-conjugated Phalloidin (C). The panel D shows the merged images counterstained with DAPI. Scale bar, 50 µm.

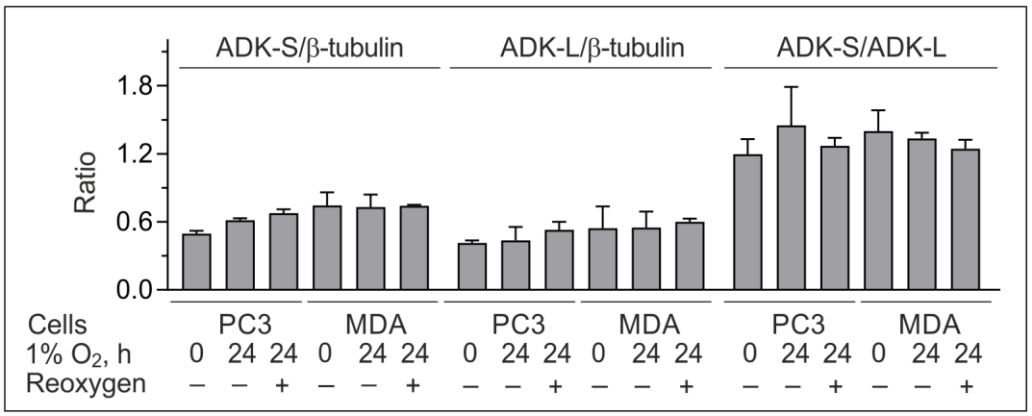

Fig. S3. The effect of hypoxia on the distribution of ADK isoforms in cancer cells. PC3 and MDA-MB-231 (*MDA*) cells were subjected to 24-hour hypoxia with or without subsequent 1-hour reoxygenation. The expression levels of cytosolic (ADK-S) and nuclear (ADK-L) isoforms of ADK were determined in the cell lysates, by using Western blot analysis (see Fig. 6B). For each experiment, the blots were probed with an anti-β-tubulin mAb to normalize for protein loading. Mean intensities of the bands were quantified using ImageJ from duplicate analyses.

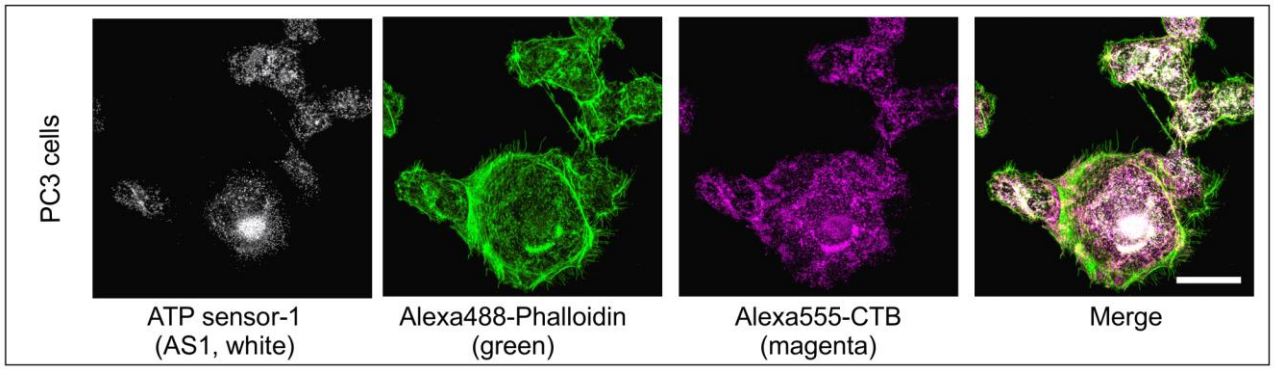

Fig. S4. Visualization of putative ATP stores in PC3 prostate carcinoma cells. PC3 cells grown on coverslips were co-stained with a fluorescent ATP-sensing dye, AS1, in combination with a cell-surface marker Alexa555-CTB and actin-binding drug Alexa488-Phalloidin, as indicated. Computer reconstructions of these signals from serial confocal images along the *z*-axis are shown in Supplementary Movie S1. Scale bar, 40 µm.

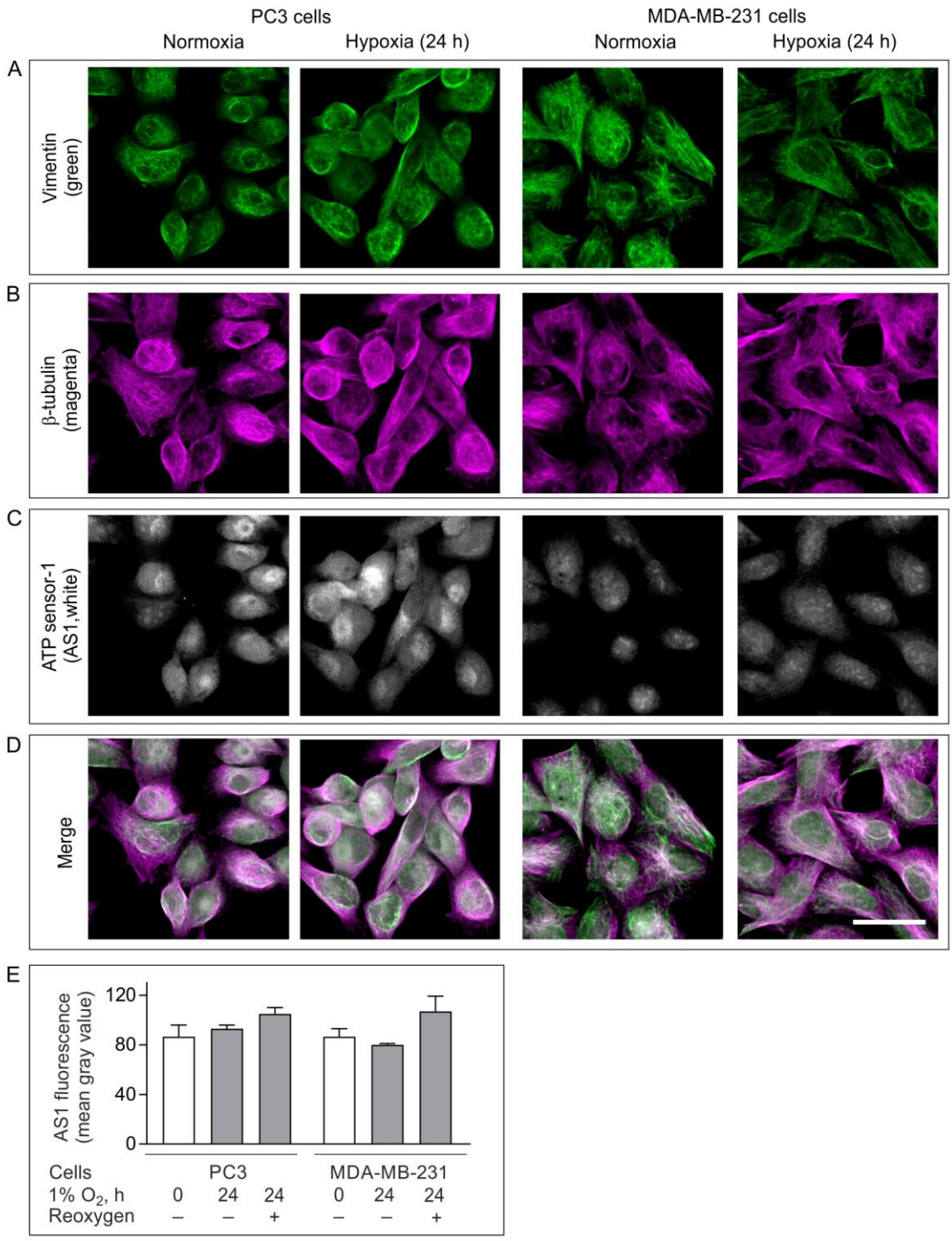

Fig. S5. Characterization of putative ATP stores and microtubular and filamentous networks in normoxic and hypoxic cancer cells. PC3 and MDA-MB-231 cells were incubated for 24 hours in the incubator with 21% O_2 (*"Normoxia"*) or in the hypoxic chamber containing 1% O_2 ("*Hypoxia*"). The treated cells were co-stained with anti-vimentin (A) and anti-β-tubulin (B) antibodies, together with a fluorescent ATP-sensing dye AS1 (C). The panel D shows the merged images. Scale bar, 40 µm. (D) The amount of AS1-specific fluorescence in normoxic and hypoxic cells was quantified from respective images using ImageJ software, and the results are presented as mean gray values (mean ± SEM; n=3).

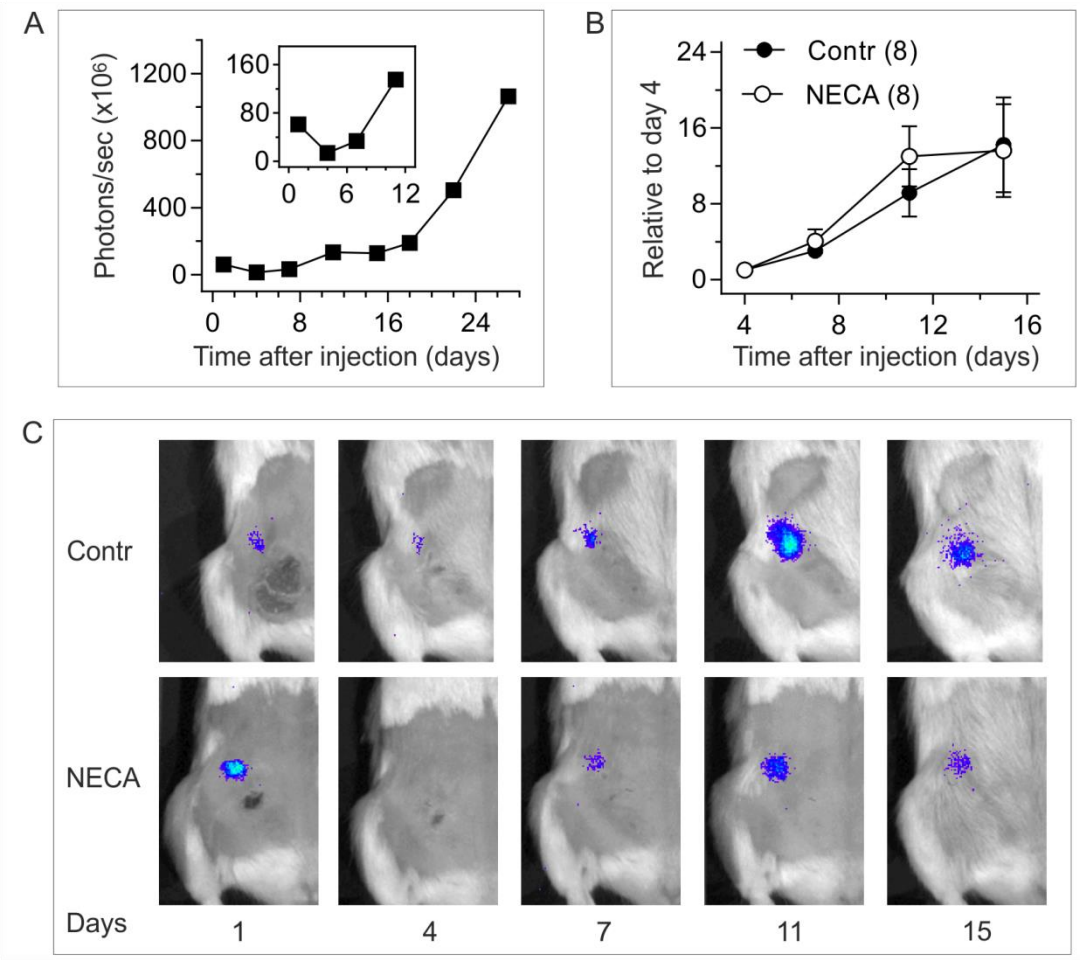

Fig. S6. Pre-treatment of cancer cells with NECA did not affect their growth *in vivo*. (A) Human MDA-MB-231-luc-D3H2LN cells were pre-treated without (*Contr*) or with a non-selective adenosine receptor agonist NECA (10 μM), and subsequently injected into the mammary fat pad of female SCID mice on day 0. The rate of tumor growth was monitored by IVIS imaging after a substrate D-luciferin injection, and panel A shows raw bioluminescence values (expressed as photons/sec) for representative individual tumor. Tumor-bearing mice were scanned on days 1, 4, 7, 11, and 15 to monitor the growth of vehicle- and NECA-treated tumors. Panels B and C display time-course of the bioluminescence signals (normalized relative to day 4) and representative IVIS images of control and treatment mice, respectively. The numbers of animals in each group are shown in parentheses.

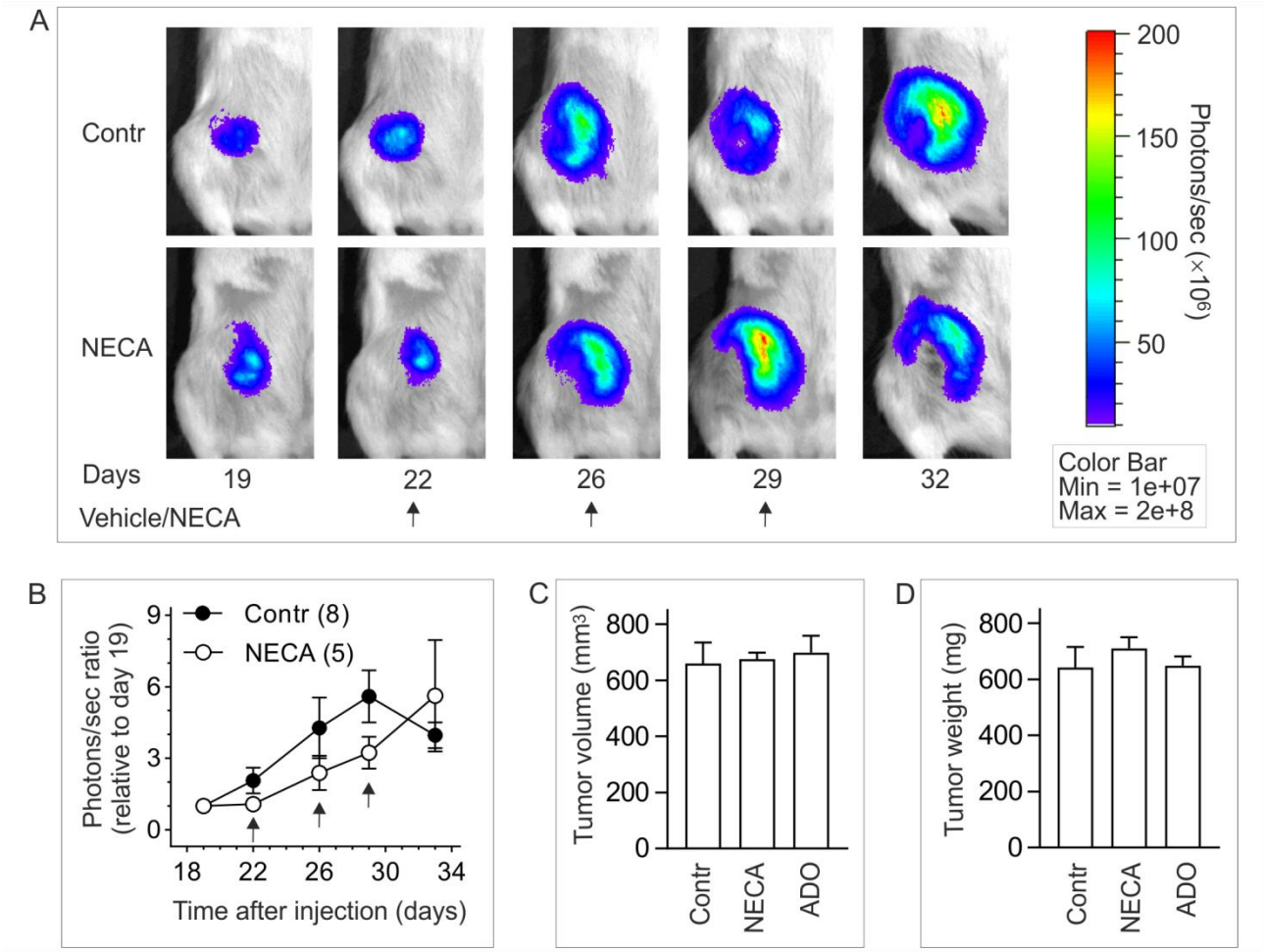

Fig. S7. The effect of ADO and NECA on the growth of established tumors in xenograft breast cancer model. (A) Human MDA-MB-231-luc-D3H2LN cells were injected into the mammary fat pad of female SCID mice and grown for three weeks. The established primary mammary tumors were treated on days 22, 26 and 29 with 50 µl of NECA (10 µM) or equal volumes of PBS containing 0.02% DMSO (*Contr*). (A) The panels show bioluminescence signals over time for representative individual tumors with intratumoral treatments pointed out by arrows. The images show photon flux from bioluminescence on a pseudocolor scale, with red and blue representing the highest and lowest values, respectively. (B) The imaging data were quantified, corrected for background signal, and normalized relative to day 19. The numbers of animals in each group are shown in parentheses. Tumor-bearing mice were euthanized on day 32, and the tumors excised. The volume and weight of the control vehicle-treated tumors and also tumors treated with ENHA and ADO (see "Experiment 2" in Fig. 8) were measured by using an electronic caliper (C) and precision scales (D), respectively (mean ± SEM, n=5-10).

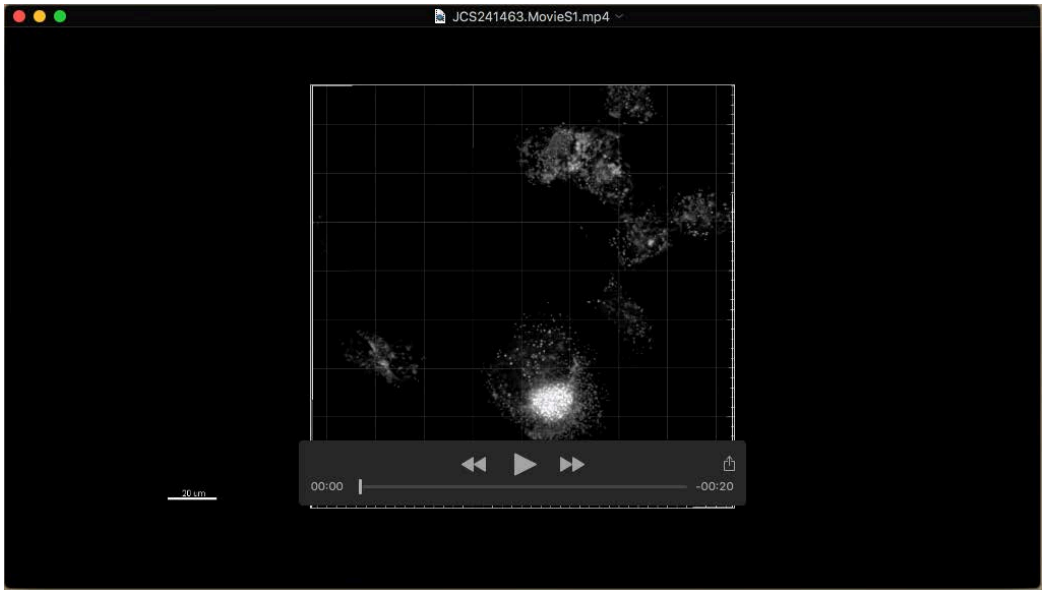

Movie 1. Characterization of putative ATP stores in cancer cells. PC3 prostate cancer cells were co-stained with a fluorescent ATP-sensing dye AS1 (white), together with a cell surface marker Alexa Fluor®555-CTB (magenta) and actin-binding drug Alexa Fluor®488-Phalloidin (green). Serial confocal images along the *z*-axis were captured using a 3i spinning disk confocal microscope CSU-W1 with Plan-Neofluar oil 63×/1.4 objective (Carl Zeiss), followed by their three-dimensional reconstruction using Imaris 8.4 software (Bitplane). For single channel view of maximum z-stack projection, see Supplementary Fig. S4.